

# Silhouette-Driven Instance-Weighted $k$ -means

Aggelos Semoglou<sup>1,2\*</sup>, Aristidis Likas<sup>3</sup> and John Pavlopoulos<sup>1,2</sup>

<sup>1\*</sup> Athens University of Economics and Business, Greece.

<sup>2</sup>Archimedes, Athena Research Center, Greece.

<sup>3</sup> University of Ioannina, Greece.

\*Corresponding author(s). E-mail(s): [a.semoglou@athenarc.gr](mailto:a.semoglou@athenarc.gr);

Contributing authors: [arly@cs.uoi.gr](mailto:arly@cs.uoi.gr); [annis@aueb.gr](mailto:annis@aueb.gr);

## Abstract

Clustering is a fundamental unsupervised learning task with applications across a wide range of domains. Popular algorithms such as  $k$ -means are efficient and widely used, but can be sensitive to outliers, ambiguous boundary points, and heterogeneous cluster geometry, which may distort centroid estimates and yield suboptimal partitions. We introduce K-SIL, a silhouette-driven  $k$ -means variant that, at each iteration, weights points using a centroid-margin proxy for the silhouette score, emphasizing confidently assigned instances while down-weighting borderline or noisy regions. Centroid updates take the form of a softmax-weighted mean, and an adaptive temperature automatically calibrates the sharpness of the weight distribution using a cluster-balanced, macro-averaged, silhouette criterion. Under standard separation conditions, we establish a local convergence result for the induced weighted centroid updates. Experiments on 15 real-world datasets spanning tabular, biomedical, text, and image representations show consistent gains in internal validation metrics and typical improvements in external validation metrics over  $k$ -means and competitive instance-weighted baselines.

**Keywords:** unsupervised learning, clustering, weighted  $k$ -means, silhouette score

## 1 Introduction

Clustering, the process of organizing data into meaningful groups, is a cornerstone of unsupervised learning with broad applications in pattern recognition and data mining [1, 2]. Among clustering algorithms,  $k$ -means [3] remains widely adopted due to its simplicity, scalability, and strong performance when clusters are well separated [4].

However, the same property that makes  $k$ -means efficient, updating each centroid as an unweighted mean of its assigned points, can make it sensitive in realistic settings [5]. Under uncertain boundary assignments, noise and outliers, or heterogeneous within-cluster structure, the arithmetic mean can be pulled toward ambiguous regions, propagating early mistakes and yielding suboptimal partitions [6]. This motivates a long line of work on robust and weighted variants of  $k$ -means, where each sample’s influence is adjusted to reduce sensitivity to unreliable observations [7].

A central challenge in instance-weighted centroid methods is deciding *which* points are reliable and *how strongly* they should influence centroid updates. Many approaches rely on density scores and outlier estimates [8], or introduce additional modeling assumptions, which may increase complexity or require careful tuning. In contrast,  $k$ -means iterations already compute a natural geometric signal of assignment confidence: distances to the assigned centroid and to competing centroids. This perspective suggests the following research question:

*How can geometric signals of assignment confidence be converted, at each iteration, into a principled weighting distribution that shapes centroid updates, while preserving the efficient centroid-based structure of  $k$ -means?*

To address this research question we introduce K-SIL, a silhouette-driven, instance-weighted  $k$ -means variant that converts centroid-distance confidence signals into a weighting mechanism. At each iteration, K-SIL computes for every point a centroid-based approximation of the silhouette score [9–11]. These scores are then mapped through an exponential transformation, producing positive instance weights that define a softmax-weighted centroid update, a convex combination of the points in each cluster. This acts like a within-cluster attention mechanism, giving more influence to confidently assigned points. As centroids move, the weights are recomputed, yielding an iterative reweighting process that increasingly emphasizes well-separated points while reducing the influence of ambiguous boundary points.

A practical consideration is calibrating the sharpness of the weighting. Overly flat weights recover standard  $k$ -means, while overly peaked weights can make updates excessively selective. To handle this trade-off without manual tuning, we introduce an adaptive temperature that adjusts the reweighting based on changes in a cluster-balanced (macro-averaged) silhouette score [12] across iterations. When clustering quality improves, the temperature sharpens the weights, as the geometry becomes more reliable and confident points can be emphasized; when it plateaus or falls, it flattens the weights to allow more exploratory updates.

We validate K-SIL with both theory and experiments. Our theoretical analysis studies its local behavior in well-separated regimes and shows local convergence of the induced weighted centroid iterations. Empirically, on a diverse set of 15 real-world datasets, K-SIL consistently improves internal clustering quality (e.g., silhouette, Davies–Bouldin) and typically increases external validation metrics (e.g., NMI, ARI) compared to standard  $k$ -means and other instance-weighted baselines.

Our code on K-SIL is available at: <https://github.com/semoglou/ksil-clustering>.

## 2 Related work

### Centroid-based clustering.

Clustering algorithms include centroid-based partitioning (e.g.,  $k$ -means) [3], density-based methods (e.g., DBSCAN) [13], hierarchical clustering [14], model-based approaches (e.g., GMMs) [15], and spectral techniques [16]. In this study, we focus on improving centroid-based partitioning via instance-level weighting derived from internal confidence signals.  $k$ -means alternates between nearest-centroid assignment and updates centroids by unweighted means, minimizing within-cluster variance. While efficient, it is sensitive to initialization, noise, and outliers. Initialization methods, such as  $k$ -means++ [17] and seeding schemes [18] improve stability, while variants such as global  $k$ -means [19, 20] aim to avoid poor local minima. However, these approaches typically preserve the same mean-based centroid update, so they do not directly control the influence of unreliable points during optimization.

### Silhouette and internal validation.

Internal validation indices provide feedback on cluster cohesion and separation (e.g., Davies–Bouldin, Calinski–Harabasz) [21] without ground-truth cluster labels. Among them, the silhouette coefficient [10, 11] assigns each point a score by contrasting its average intra-cluster dissimilarity with its minimum average inter-cluster dissimilarity. Computing silhouette scores is expensive due to their reliance on pairwise distances, motivating simplified and centroid-based approximations that preserve the same intuition while scaling efficiently [9]. Beyond evaluation, silhouette has also motivated refinement methods and objectives that explicitly incorporate silhouette-based criteria [22, 23]. Recent work further shows that the choice of silhouette aggregation, micro (global) vs. macro (per-cluster), can substantially affect outcomes, with macro-averaging being particularly suitable when one aims to control cluster-level behavior [12].

### Weighted $k$ -means variants.

Weighted variants of  $k$ -means address the limitations of the unweighted mean update by modulating either feature importance or instance influence. Feature-weighted methods (e.g., WK-Means and EWKM) [24, 25] learn per-feature weights to reduce the effect of irrelevant dimensions, while related schemes such as AWA [26] use variance-driven weighting to improve robustness under noisy features. Recent feature-weighted variants also use silhouette to update dimension weights during  $k$ -means iterations (e.g., WKBSC) [27]. More closely related to our setting are instance-weighted approaches, which control how strongly individual points influence centroid updates. A prominent line of work derives weights from outlier analysis estimated via local neighborhood structure, as in LOF-based and iterative iLOF-based  $k$ -means [8, 28]. Similarly, OWKMeans introduces an object-weighted  $k$ -means objective, updating per-point weights and penalties from distance and silhouette-width signals, with higher penalties for poorly separated or overlapping points [29]. K-SIL follows this line by turning silhouette-based confidence into within-cluster weighting distributions that are adaptively sharpened over iterations and directly shape the centroid updates.

## 3 Methodology

### 3.1 Data and notation

Let  $\mathcal{X} = \{x_1, x_2, \dots, x_n\} \subset \mathbb{R}^d$  be fixed data points. A clustering into  $k \in \mathbb{N}$  ( $k > 1$ ) distinct clusters  $\{C_1, C_2, \dots, C_k\}$  is described by (i) the corresponding centroids  $\mu$ :

$$\mu = (\mu_1, \mu_2, \dots, \mu_k) \in (\mathbb{R}^d)^k \cong \mathbb{R}^{kd}, \quad (1)$$

and (ii) the cluster labels (indices)  $c(i)$  for each data point  $x_i \in \mathcal{X}$ :

$$c : \{1, \dots, n\} \rightarrow \{1, \dots, k\}, \quad c(i): \text{the cluster index for point } x_i \in \mathcal{X}. \quad (2)$$

Given centers  $\mu$ , we use the nearest-centroid assignment:

$$c(\mu)(i) \in \arg \min_{1 \leq j \leq k} \|x_i - \mu_j\| \quad \forall x_i \in \mathcal{X} \quad (3)$$

with a fixed and deterministic tie-breaking rule (e.g. smallest index). We write the index set of cluster  $j$  as  $C_j(\mu) = \{i : c(\mu)(i) = j\}$ , and its size as  $n_j(\mu) = |C_j(\mu)|$ .

### 3.2 Centroid initialization

Given a prescribed number of clusters  $k$ , K-SIL starts from an initial set of centroids  $\mu_0 = (\mu_{0,1}, \dots, \mu_{0,k}) \in (\mathbb{R}^d)^k$ . In practice,  $\mu_0$  can be obtained either by selecting  $k$  data points at random from  $\mathcal{X}$  or by using a more structured seeding strategy such as  $k$ -means++ initialization. Once  $\mu_0$  is chosen, the initial labels are assigned by the nearest-centroid rule in Eq. 3. The subsequent sections (§3.3–§3.6) describe how, given current centroids and cluster labels, K-SIL computes silhouette scores, instance weights, and updates centroids.

### 3.3 Centroid-margin silhouette proxy

At each iteration of K-SIL, given the current centroids and labels, we first compute silhouette-based scores for all points. These scores are then used (i) to define silhouette-based instance weights (§3.4), and (ii) to provide a global measure of clustering quality that controls how strongly K-SIL emphasizes high-confidence points in subsequent updates (§3.5).

Classical silhouette scores are defined using average intra- and inter-cluster distances between points. For efficiency, K-SIL uses a centroid-based proxy: each point’s silhouette is computed solely from its distance to cluster centroids. Given centers  $\mu = (\mu_1, \mu_2, \dots, \mu_k)$  and the associated labels  $c(\mu)$ , we define for each point  $x_i \in \mathcal{X}$  its intra-cluster distance proxy (own centroid distance)  $a_i = a_i(\mu)$  and its inter-cluster distance proxy (nearest other centroid distance)  $b_i = b_i(\mu)$ :<sup>1</sup>

$$a_i(\mu) = \|x_i - \mu_{c(\mu)(i)}\|, \quad b_i(\mu) = \min_{j \neq c(\mu)(i)} \|x_i - \mu_j\|. \quad (4)$$

---

<sup>1</sup>In the standard silhouette definition,  $a_i$  is the average distance from  $x_i$  to all other points in its assigned cluster, and  $b_i$  is the minimum (over clusters  $j \neq c(i)$ ) of the average distance from  $x_i$  to points in cluster  $j$ .

The per-point silhouette proxy is then:

$$s_i(\mu) = \frac{b_i(\mu) - a_i(\mu)}{\max\{a_i(\mu), b_i(\mu)\}}. \quad (5)$$

In our centroid-distance proxy,  $s_i(\mu)$  is best understood as a normalized centroid–margin: it compares the distance from  $x_i$  to its assigned centroid with the distance to the nearest other centroid. Values  $\approx 1$  indicate points that lie well inside their assigned cluster, whereas values near 0 correspond to points close to a centroid decision boundary. Moreover *the proxy scores are constrained to be nonnegative*. By the assignment rule in Eq. 3,  $a_i(\mu) = \|x_i - \mu_{c(\mu)(i)}\| \leq \|x_i - \mu_j\| \quad \forall j$ , and in particular  $a_i(\mu) \leq b_i(\mu)$ . We therefore have  $\max\{a_i(\mu), b_i(\mu)\} = b_i(\mu)$  and thus  $s_i(\mu) = \frac{b_i(\mu) - a_i(\mu)}{b_i(\mu)} \in [0, 1]$ . If  $a_i(\mu) > b_i(\mu)$  were to occur, then  $c(\mu)(i)$  could not be a minimizer in Eq. 3, which gives a contradiction. Additionally, we aggregate the pointwise silhouette scores into a macro-averaged, cluster-level score by averaging the mean silhouette of each cluster ( $n_j \geq 1$ ; see empty-cluster re-initialization strategy in Appendix B):

$$S(\mu) = \frac{1}{k} \sum_{j=1}^k \frac{1}{n_j(\mu)} \sum_{c(\mu)(i)=j} s_i(\mu) \in [0, 1]. \quad (6)$$

This macro-averaging is particularly useful in the presence of unbalanced cluster sizes. Unlike the global mean silhouette score  $\frac{1}{n} \sum_{x_i} s_i$  (the standard micro-averaged score used by `sklearn`), which is dominated by large clusters,  $S(\mu)$  gives each cluster equal weight in the overall score. As a result, it is sensitive to poorly separated or low-quality clusters even when they contain relatively few points, and thus provides a more balanced measure of clustering quality for guiding the adaptive steps of K-SIL (§3.5).

### 3.4 Instance weights and centroid update

Given centers  $\mu$  and a temperature parameter  $\tau > 0$  (§3.5), K-SIL uses the silhouette scores  $\{s_i(\mu)\}$  to define instance weights  $w_i$  and update the cluster centroids as weighted means. Each instance  $x_i \in \mathcal{X}$  is assigned a silhouette-based weight:

$$w_i(\mu, \tau) = \exp\{\tau s_i(\mu)\} > 0. \quad (7)$$

Points with higher silhouette  $s_i(\mu)$  (i.e. better cluster fit) thus receive exponentially higher weights, while ambiguous or poorly fitted points are down-weighted. Given centroids  $\mu = (\mu_j)_{j=1}^k$  (Eq. 1), the (updated) weighted centroid of cluster  $j$ ,  $\mu_j$ , is:

$$H_j(\mu, \tau) = \frac{\sum_{i \in C_j(\mu)} w_i(\mu, \tau) x_i}{\sum_{i \in C_j(\mu)} w_i(\mu, \tau)} = \text{softmax} \left( \tau \left[ s_i(\mu) \right]_{i \in C_j(\mu)} \right)^\top \left[ x_i \right]_{i \in C_j(\mu)}, \quad (8)$$

where the softmax is taken over the index set  $C_j(\mu)$  and  $[x_i]_{i \in C_j(\mu)}$  denotes the stacked vector of points in cluster  $j$ . Thus,  $H_j(\mu, \tau)$  is a convex combination of the points in  $C_j(\mu)$ , with weights proportional to  $\exp\{\tau s_i(\mu)\}$  and normalized to one via softmax.

Geometrically, the silhouette scores  $s_i(\mu)$  quantify how well each point fits its assigned cluster, and the softmax transformation turns these scores into a probability distribution within each cluster (over  $C_j(\mu)$ ). This is analogous to within-cluster attention: points with high silhouette receive most of the probability mass and therefore “pull” the centroid  $H_j(\mu, \tau)$  toward well-supported regions of the cluster, while low-silhouette boundary or misclustered points have little influence. This makes the centroid update more robust than an unweighted mean and allows K-SIL to focus its updates on high-confidence points. We collect the cluster-wise centroid updates into:

$$H(\mu, \tau) = (H_1(\mu, \tau), H_2(\mu, \tau), \dots, H_k(\mu, \tau)) \in \mathbb{R}^{kd}, \quad (9)$$

which defines the centroid update step of one K-SIL iteration for a temperature  $\tau$ .

### 3.5 Temperature parameter

The temperature  $\tau > 0$  controls the sharpness of the silhouette-based weights in Eq. 7. For small  $\tau$ , we have  $\exp\{\tau s_i(\mu)\} \approx 1$  for all  $i$ , so the weights  $w_i(\mu, \tau)$  are nearly uniform and  $H_j(\mu, \tau)$  is close to the standard (unweighted) cluster mean. As the temperature  $\tau$  increases, the softmax in Eq. 8 becomes more peaked: points with larger silhouette  $s_i(\mu)$  (well inside the cluster) receive disproportionately large weights, while low-silhouette points contribute very little. In the limit of large  $\tau$ , the centroid update is dominated by the highest-silhouette points in each cluster. Thus,  $\tau$  acts as a “focus” parameter that interpolates between uniform averaging and an update driven almost exclusively by the most confidently assigned points (Fig. 1).

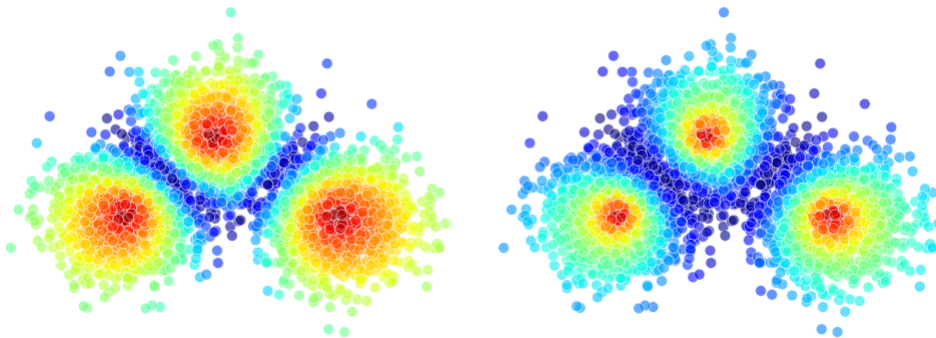


**Fig. 1:** Effect of temperature  $\tau$  on weights (Eq. 7), on synthetic data ( $k = 3$ ). **Left:**  $\tau = 0.2$  (flatter weighting). **Right:**  $\tau = 2$  (more peaked weighting) ( $\uparrow$  red,  $\downarrow$  blue).

In K-SIL, the temperature is initialized at a neutral value,  $\tau_0 = 1$  or  $2$  (Appendix C.1 describes an optional rule selecting  $\tau_0 \in \{1, 2\}$  from the initial  $s_i(\mu_0)$  distribution), and then updated adaptively based on the evolution of the macro silhouette  $S(\mu)$  (Eq. 6) across iterations. Let  $S_t = S(\mu_t)$  denote the macro silhouette at iteration  $t$ . For  $t \geq 1$  we first compute a normalized score drift by comparing  $S_t$  and  $S_{t-1}$ :

$$\tilde{r}(S_t, S_{t-1}) = \frac{S_t - S_{t-1}}{1 - S_{t-1} + \varepsilon}, \quad \varepsilon > 0 \text{ small for stability.} \quad (10)$$

Since  $S_t \in [0, 1]$  (§3.3), the denominator  $1 - S_{t-1}$  approximately measures the remaining “headroom” to the best possible value (1). Thus,  $\tilde{r}(S_t, S_{t-1}) (< 1)$  encodes the signed change in  $S_t$  relative to the largest improvement still possible from  $S_{t-1}$ : values  $\tilde{r}(S_t, S_{t-1}) \approx 1$  correspond to improvements that nearly exhaust this headroom, while small  $|\tilde{r}(S_t, S_{t-1})|$  indicate only minor changes. To prevent overly large temperature reactions when  $S_t$  drops, we use  $R(S_t, S_{t-1}) = \max\{-1, \tilde{r}(S_t, S_{t-1})\} \in [-1, 1]$ . Next, we fix a temperature lower bound  $\tau_{\min} > 0$  and define an upper bound  $\tau_{\max}(t)$  per iteration using the current cluster sizes. Let  $n_j(\mu_t) = |C_j(\mu_t)|$  be the size of cluster  $j$  at iteration  $t$  (assuming  $n_j(\mu_t) \geq 3 \forall j, t$ , see Appendix B), and set  $m_{\max}(\mu_t) = \max_{1 \leq j \leq k} n_j(\mu_t)$ , the size of the largest cluster at iteration  $t$ . Within a cluster, weight ratios scale exponentially:  $w_i/w_h = \exp\{\tau(s_i - s_h)\}$  for  $x_i, x_h$  in the same cluster. To keep this contrast from becoming excessively large as cluster size grows, we cap  $\tau$  using a worst-case reference configuration in a cluster of size  $m$ , where one point has  $s = 1$  and the remaining  $m - 1$  points have  $s = 0$ . In this configuration the cluster’s mean silhouette is  $1/m$ , so the best point exceeds the mean by  $1 - 1/m$ . We choose  $\tau_{\max}$  so that the corresponding weight spread relative to this mean is at most  $m^2$  (a quadratic cap that prevents the exponentiated weights from becoming excessively large as  $m$  grows):  $\exp\left\{\tau\left(1 - \frac{1}{m}\right)\right\} \leq m^2$ , which yields  $\tau \leq \frac{2 \log m}{(m-1)/m}$ . We therefore set  $\tau_{\max}(t)$  using  $m = m_{\max}(\mu_t)$ , i.e., the bound is calibrated by the largest cluster size, and define:

$$\tau_{\max}(t) = \frac{2 m_{\max}(\mu_t) \log m_{\max}(\mu_t)}{m_{\max}(\mu_t) - 1}. \quad (11)$$

This cap is a stabilization safeguard on the temperature dynamics, and it scales only logarithmically with  $m_{\max}(\mu_t)$ . The raw temperature update is a multiplicative, exponentiated-gradient step:

$$\tau_{t+1}^{\text{raw}} = \tau_t \exp\{\eta R(S_t, S_{t-1})\}, \quad (12)$$

where  $\eta$  is a learning rate parameter (default: 0.2; Appendix Fig. C1 shows that, under the temperature bounds, performance is largely insensitive to  $\eta$  over  $\{0.1, 0.2, 0.3\}$ , making further tuning typically unnecessary). Thus  $\tau_t e^{-\eta} \leq \tau_{t+1}^{\text{raw}} \leq \tau_t e^{\eta}$  and the new temperature  $\tau_{t+1}$  is obtained by clipping  $\tau_{t+1}^{\text{raw}}$ , so that  $\tau_{\min} \leq \tau_{t+1} \leq \tau_{\max}(t) \forall t$ . In regimes where the cluster sizes stabilize,  $\tau_{\max}(t)$  also stabilizes, and  $\tau$  remains in a fixed interval  $[\tau_{\min}, \tau_{\max}^*]$ . This adaptive scheme has an intuitive interpretation: if  $S_t$  increases, the algorithm gradually raises  $\tau$ , sharpening the weights and letting the centroids focus more on high-quality points. If  $S_t$  decreases, the algorithm lowers  $\tau$ , flattening the weights and allowing for broader, more exploratory centroid updates. We summarize this update as an abstract map:

$$\Psi_{\eta}(\tau_t, S_t, S_{t-1}) = \tau_{t+1} = \text{clip}_{[\tau_{\min}, \tau_{\max}(t)]}[\tau_t \exp\{\eta R(S_t, S_{t-1})\}]. \quad (13)$$

### 3.6 Convergence and stopping criterion

K-SIL alternates between (i) computing centroid-proxy silhouettes  $s_i(\mu)$  and the macro averaged silhouette score  $S(\mu)$  (§3.3, Eqs. 5–6), (ii) updating the temperature  $\tau$  using the adaptive rule  $\Psi_\eta$  (§3.5, Eq. 10–13), (iii) updating centroids using the weighted map  $H$  (§3.4, Eqs. 8–9), and (iv) assigning labels with the nearest-centroid  $c$  (§3.1, Eq. 3) with a deterministic tie-breaking; if any cluster becomes empty, its centroid is re-initialized using the safeguard in Appendix B. These updates (outlined in Alg. 1) are repeated until either a maximum number of iterations  $T_{\max}$  is reached (default  $T_{\max} = 100$ ) or when the centroids stabilize. Specifically, letting  $\mu_{t,j}$  be a centroid  $j$  at iteration  $t$ , we compute the average centroid movement:

$$\Delta_t = \frac{1}{k} \sum_{j=1}^k \|\mu_{t+1,j} - \mu_{t,j}\|, \quad (14)$$

and declare convergence when  $\Delta_t < \text{tol}$  for a tolerance level  $\text{tol} > 0$  ( $10^{-4}$  in default).<sup>2</sup>

---

#### Algorithm 1 K-SIL clustering

---

**Require:** Dataset  $\mathcal{X} = \{x_i\}_{i=1}^n \subset \mathbb{R}^d$ , number of clusters  $k > 1$ , learning rate  $\eta > 0$  (default: 0.2), maximum number of iterations  $T_{\max}$  (default: 100), centroid movement tolerance (convergence threshold)  $\text{tol}$  (default:  $10^{-4}$ )

**Ensure:** Cluster centroids  $\mu$  and labels  $c$

**Initialization** (§3.2)

Choose initial centroids  $\mu_0 = (\mu_{0,1}, \dots, \mu_{0,k})$  (e.g. random points in  $\mathcal{X}$ )

Assign initial labels  $c_0 \leftarrow c(\mu_0)$  using nearest-centroid rule (Eq. 3)

Set initial temperature  $\tau_0 \leftarrow 1.0$  (Appendix C.1) and  $S_{-1} \leftarrow \text{None}$

**for**  $t = 0, 1, \dots, T_{\max} - 1$  **do**

**Silhouette computation** (§3.3)

Given  $(\mu_t, c_t)$ , compute  $s_i(\mu_t)$  and  $S_t = S(\mu_t)$  (Eqs. 4–6)

**if**  $S_{t-1} = \text{None}$  **then** set  $S_{t-1} \leftarrow S_t$  so the first update uses  $S_t = S_{t-1}$

**Temperature update** (§3.5)

Update temperature  $\tau_{t+1} \leftarrow \Psi_\eta(\tau_t, S_t, S_{t-1})$  (Eq. 13)

**Weight computation and centroid update** (§3.4)

Compute weights  $w_i(\mu_t, \tau_{t+1}) \leftarrow \exp\{\tau_{t+1} s_i(\mu_t)\}$  for all  $i$  (Eq. 7)

Update centroids by the weighted centroid map  $\mu_{t+1} \leftarrow H(\mu_t, \tau_{t+1})$  (Eqs. 8–9)

Reassign labels  $c_{t+1} \leftarrow c(\mu_{t+1})$  using nearest-centroid assignment (Eq. 3)

**if** any cluster is empty **then** re-initialize its centroid (as in Appendix B)

**Convergence check** (§3.6)

Compute the average centroid movement  $\Delta_t \leftarrow \frac{1}{k} \sum_{j=1}^k \|\mu_{t+1,j} - \mu_{t,j}\|$  (Eq. 14)

**if**  $\Delta_t < \text{tol}$  **then return** centroids  $\mu_{t+1}$  and labels  $c_{t+1}$

Set  $S_{t-1} \leftarrow S_t$  for the next iteration

**end for**

**return** final centroids  $\mu_{T_{\max}}$  and labels  $c_{T_{\max}}$

---

<sup>2</sup>In all experiments reported (§5.2), K-SIL satisfied the centroid-stabilization criterion  $\Delta_t < \text{tol}$  before reaching the iteration cap  $T_{\max}$  (Fig. 3; Appendix C Figs. C3–C6). Thus,  $T_{\max}$  serves only as a safeguard to guarantee termination in pathological cases.

## 4 Theoretical Analysis

### 4.1 Local convergence

We study the local behavior of K-SIL around a well-separated configuration. Recall that one iteration updates  $\tau_{t+1} = \Psi_\eta(\tau_t, S_t, S_{t-1})$ ,  $\mu_{t+1} = H(\mu_t, \tau_{t+1})$ ,  $S_t = S(\mu_t)$ , (§3.6, Alg. 1) with labels given by nearest-centroid assignment  $c(\mu_t)$  (Eq. 3). We list Assumptions A.1, A.2 and Lemmas L.1–L.4 used in our analysis, along with the local convergence theorem. Full proofs and detailed derivations are provided in Appendix A.

**Norm.** For  $\mu \in \mathbb{R}^{kd}$  (Eq. 1) we use the block-max norm  $\|\mu\|_{\infty,2} = \max_{1 \leq j \leq k} \|\mu_j\|_2$ .

Fix centers  $\mu_\star \in \mathbb{R}^{kd}$  and let  $c_\star = c(\mu_\star)$  denote the induced nearest-centroid labels. Throughout the local analysis we assume the induced clustering has no empty clusters and we study iterates initialized in a neighborhood of  $\mu_\star$ .

**A.1 (Geometric separation at  $\mu_\star$ ).** There exists  $r > 0$  such that for each cluster  $j$  and all  $i$  with  $c_\star(i) = j$ ,  $\|x_i - \mu_{\star,j}\| \leq r$ , and  $\|\mu_{\star,j} - \mu_{\star,\ell}\| \geq 5r \quad \forall j \neq \ell$ . Thus, each cluster lies inside a ball of radius  $r$  around its centroid, and distinct centroids are at least  $5r$  apart. This is an idealized but standard local margin assumption used to simplify the analysis by ruling out nearly overlapping clusters near  $\mu_\star$ .

**A.2 (Local bounded-temperature).** We analyze the dynamics in a neighborhood where: (i)  $\tau$  remains bounded:  $\tau_t \in [\tau_{\min}, \bar{\tau}]$  for all  $t$ , for some  $\bar{\tau} > 0$ ; (ii) the drift lower clipping is inactive along iterates, i.e.  $\tilde{r}(S_t, S_{t-1}) > -1$  so that  $R(S_t, S_{t-1}) = \tilde{r}(S_t, S_{t-1})$ ; (iii) the “headroom” denominator is bounded below: there exists  $\alpha > 0$  such that  $1 - S_t + \epsilon \geq \alpha$  for all  $t$ . ((i) is ensured in practice by Eq. 13; (ii)–(iii) are mild local regularity conditions ruling out saturation of the drift normalization.)

**L.1 (Stability near  $\mu_\star$ ).** Let  $U_\mu := \{\mu \in \mathbb{R}^{kd} : \|\mu - \mu_\star\|_{\infty,2} \leq r\}$  be a neighborhood of  $\mu_\star$ . Under A.1, for every  $\mu \in U_\mu \Rightarrow c(\mu) = c_\star$ . Moreover,  $H(\mu, \tau) \in U_\mu \quad \forall \tau \geq 0$ .

**L.2 (Silhouette Lipschitz bound).** For  $\mu, \mu' \in U_\mu$ , each  $s_i(\mu)$  and  $S(\mu)$  satisfy  $|s_i(\mu) - s_i(\mu')| \leq L_s \|\mu - \mu'\|_{\infty,2}$ ,  $|S(\mu) - S(\mu')| \leq L_s \|\mu - \mu'\|_{\infty,2}$  with  $L_s = \frac{5}{9r}$ .

**L.3 (Softmax Lipschitz).**  $\forall u, u' \in \mathbb{R}^m$ ,  $\|\text{softmax}(u) - \text{softmax}(u')\|_1 \leq \|u - u'\|_\infty$ .

**L.4 (Lipschitz bounds for the centroid map  $H$ ).** Let  $\mu, \mu' \in U_\mu$ ,  $\tau, \tau' \geq 0$  then  $\|H(\mu, \tau) - H(\mu', \tau)\|_{\infty,2} \leq \frac{5\bar{\tau}}{9} \|\mu - \mu'\|_{\infty,2}$ , and  $\|H(\mu, \tau) - H(\mu, \tau')\|_{\infty,2} \leq r |\tau - \tau'|$ .

**Theorem 1 (Local convergence under bounded temperature).** Assume A.1, A.2 and let  $\mu_0 \in U_\mu$ . If the temperature bound  $\bar{\tau}$  satisfies  $\bar{q} = \frac{5\bar{\tau}}{9} \left(1 + \frac{e^{\bar{\tau}} - 1}{\alpha}\right) < 1$ , then the K-SIL iterates satisfy: **(i)** (local invariance)  $\mu_t \in U_\mu$  and  $c(\mu_t) = c_\star$  for all  $t$ ; **(ii)** (linear decay of step sizes) with  $d_t := \|\mu_t - \mu_{t-1}\|_{\infty,2}$ ,  $d_{t+1} \leq \bar{q} d_t$  for all  $t \geq 1$ ; **(iii)** (convergence)  $\mu_t \rightarrow \mu_\infty \in U_\mu$ ,  $S_t \rightarrow S_\infty := S(\mu_\infty)$ , and  $\tau_t \rightarrow \tau_\infty \in [\tau_{\min}, \bar{\tau}]$ ;

Under Theorem 1, labels remain fixed ( $c_t = c_\star$ ), so  $s_i(\mu_t) \rightarrow s_i(\mu_\infty)$  for each  $i$ . Since  $\mu_t \rightarrow \mu_\infty$  and  $\tau_t \rightarrow \tau_\infty$ , we have  $w_i(\mu_t, \tau_{t+1}) \rightarrow w_i(\mu_\infty, \tau_\infty)$ . In particular, the limiting centers satisfy  $\mu_{\infty,j} = \frac{\sum_{i:c_\star(i)=j} w_i(\mu_\infty, \tau_\infty) x_i}{\sum_{i:c_\star(i)=j} w_i(\mu_\infty, \tau_\infty)}$ , so  $\mu_\infty$  is a fixed point of a weighted  $k$ -means update with weights induced by the limiting silhouette-confidence profile.

## 4.2 Computational complexity

Let  $n$  be the number of points,  $d$  the dimension, and  $k$  the number of clusters. The dominant cost is computing distances from each point to the  $k$  centroids. For each  $x_i$ , we need (i) its assigned centroid distance  $\|x_i - \mu_{c(i)}\|$  and (ii) the nearest other centroid distance  $\min_{j \neq c(i)} \|x_i - \mu_j\|$ , which can be obtained by tracking the smallest and second-smallest centroid distances in one pass. This requires  $O(kd)$  work per point, hence  $O(nkd)$  per iteration. Given these distances, computing silhouettes  $s_i$  and the macro score  $S(\mu)$  is  $O(n)$ , the temperature update is  $O(k)$  (via  $m_{\max}$ ), and computing weights plus the weighted centroid update is  $O(nd)$  using per-cluster accumulators (one weighted sum and one weight sum per cluster). The label reassignment step is already available from the same distance pass (or costs another  $O(nkd)$  if recomputed from scratch). Overall, the per-iteration time is  $O(nkd)$  (dominant term), matching the standard  $k$ -means iteration order, with only constant-factor overhead. For  $T_{\max}$  iterations, the total runtime is  $O(T_{\max}nkd)$  (plus initialization, e.g. random seeding).

# 5 Empirical Validation

## 5.1 Datasets

Our empirical study consists of 15 real-world datasets from biomedical and health data, structured tabular and sensor benchmarks, natural-language corpora for topic/intent classification, and an image benchmark. All datasets are available via OpenML, UCI, and Hugging Face Datasets. We summarize each dataset by its sample size  $n$ , number of classes  $k$ , and post-preprocessing dimensionality  $d$ . **Leukemia** (LKM): cancer gene-expression profiles;  $n=72$ ,  $k=2$ ,  $d=7129$ , **Vehicle** (VCL): vehicle silhouette features;  $n=846$ ,  $k=4$ ,  $d=15$ , **Ionosphere** (INR): radar returns;  $n=351$ ,  $k=2$ ,  $d=34$ , **Mice Protein** (MIP): protein expression measurements;  $n=1,080$ ,  $k=8$ ,  $d=15$ , **Diabetes** (DBT): patient clinical measurements;  $n=768$ ,  $k=2$ ,  $d=8$ , **Wine** (WNE): wine chemistry measurements;  $n=178$ ,  $k=3$ ,  $d=13$ , **Breast Cancer** (BRC): tumor diagnostic measurements;  $n=569$ ,  $k=2$ ,  $d=30$ , **SMS Spam** (SMS): short text messages;  $n=5,574$ ,  $k=2$ ,  $d=50$ , **MINDS-14** (MDS): spoken user requests;  $n=567$ ,  $k=14$ ,  $d=50$ , **HTRU2** (HTR): pulsar candidate features;  $n=17,898$ ,  $k=2$ ,  $d=8$ , **BBC News** (BBC): news articles by topic;  $n=2,225$ ,  $k=5$ ,  $d=50$ , **R8** (RE8): Reuters newswire topics;  $n=4,941$ ,  $k=8$ ,  $d=50$ , **Banking77** (B77): banking user queries;  $n=13,083$ ,  $k=77$ ,  $d=50$ , **CLINC150** (CLC): assistant user utterances;  $n=23,800$ ,  $k=151$ ,  $d=50$ , and **STL10** (STL): natural images;  $n=13,000$ ,  $k=10$ ,  $d=100$ . Preprocessing follows the data modality. For tabular datasets we apply mean imputation when needed, followed by z-score standardization; Leukemia is treated analogously but remains high-dimensional after scaling. For the text datasets (SMS, MDS, BBC, RE8, B77, CLC), each document is embedded with MiniLM (sentence-level Transformer encoder), yielding representations that capture semantic similarity; we then project to  $d=50$  with PCA and apply  $\ell_2$  normalization. For STL, we extract CLIP (ViT-B/32) image embeddings and apply PCA to  $d=100$  followed by  $\ell_2$  normalization (Appendix C, Table C2, reports per-dataset correlation/MAE between exact `sklearn` silhouette scores and our centroid-margin

proxy §3.3, along with timing speedups). For MIP and VCL we use a UMAP representation with  $d=10$ . On these two datasets, the original feature space shows weaker alignment between silhouette-based internal separation and label-consistent external structure, which can make silhouette-based confidence weighting less informative. In the UMAP space,  $s_i(\mu)$  aligns more clearly with external agreement; this is reflected in a clearer relationship between  $s_i(\mu)$  and Hungarian-matched clustering accuracy when we compare the original space to UMAP embedding across  $s_i(\mu)$  percentiles in Fig. 2.

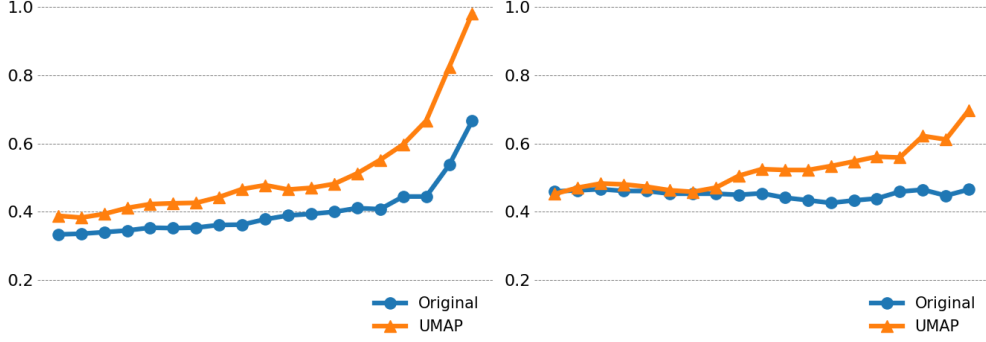


**Fig. 2:** Hungarian-matched accuracy across *top*  $s_i(\mu)$  percentiles (from a reference  $k$ -means partition), comparing the **original** feature space and the **UMAP** representation on MIP (left) and VCL (right).

## 5.2 Evaluation

### Empirical convergence.

To complement our local convergence analysis (§4.1), we empirically examine the iterative behavior of K-SIL. For each dataset in §5.1, we applied K-SIL from a random initialization with a maximum number of iterations  $T_{\max} = 100$ , and at each iteration  $t$ , we record two diagnostics: the average centroid movement  $\Delta_t$  (Eq. 14) and the Pearson correlation  $\rho_t$  between the per-instance weight vectors (Eq. 7), computed at consecutive iterates  $w(\mu_t)$  and  $w(\mu_{t+1})$ :

$$\Delta_t = \frac{1}{k} \sum_{j=1}^k \|\mu_{t+1,j} - \mu_{t,j}\|, \quad \rho_t = \text{corr}(w(\mu_{t+1}), w(\mu_t)).$$

Across datasets,  $\Delta_t$  decreases rapidly with  $t$ , while  $\rho_t$  quickly rises toward 1, indicating that the confidence weights stabilize after only a few iterations and subsequent updates mainly refine the centroids under near-fixed weights. This behavior is consistent with our theory: once assignments and weights evolve smoothly across iterations, the update behaves like a locally contractive weighted k-means step, yielding fast local convergence to a fixed point. Fig. 3 and Figs. C3–C6 in Appendix C visualize these trends (see also Appendix Fig. C7 for additional iteration diagnostics on representative datasets, including SSE and silhouette score over K-SIL iterations).

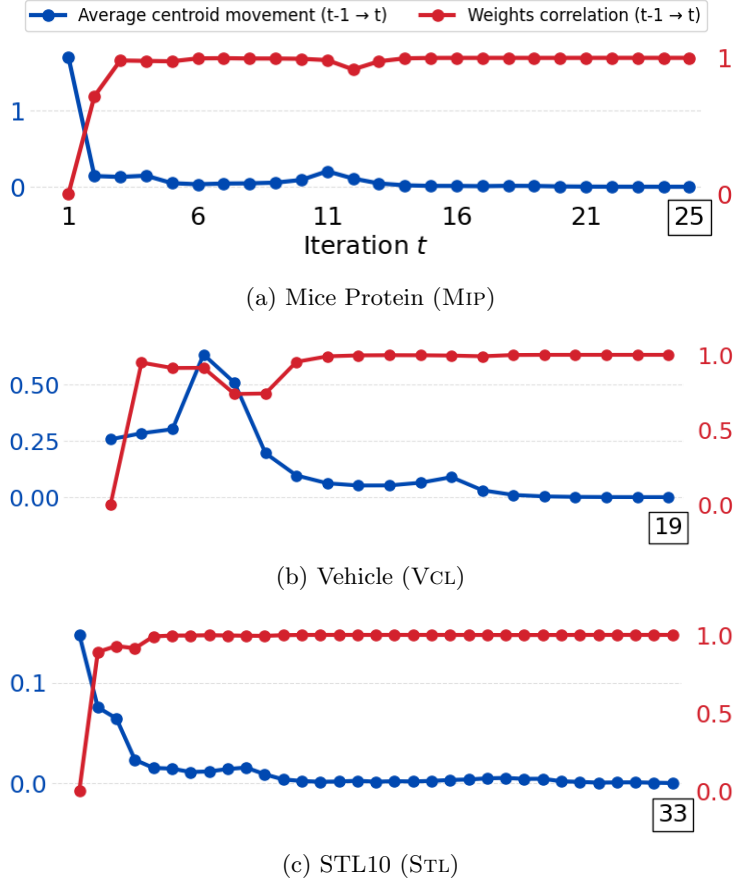


**Fig. 3:** Average centroid movement and Pearson correlation between weights across K-SIL iterations  $t$  (§5.2) for MIP, VCL and STL. The final iteration (convergence) is marked by  $\square$ . The remaining datasets (§5.1) are shown in Appendix C (Figs. C3–C6).

### Baselines and comparison.

We compare K-SIL against established instance-weighted  $k$ -means variants. As a reference, we use standard  $k$ -means. To account for outliers via density-based instance weighting, we include LOF $k$ -means and iLOF $k$ -means (iterative LOF $k$ -means) [8], two instance-weighted  $k$ -means variants in which Local Outlier Factor (LOF) scores are converted into sample weights that reduce the influence of low-density (outlying) points. LOF $k$ -means computes LOF weights once and then fits weighted  $k$ -means, while iLOF $k$ -means recomputes LOF weights within the current clusters across iterations (a cluster-wise LOF reweighting loop) before performing weighted centroid updates. We also include an object-weighting  $k$ -means baseline OW $k$ -means [29], which introduces silhouette per-point weights into the within-cluster objective; weights are obtained by rescaling each point’s silhouette width so that low-silhouette points receive larger penalties, while well-separated points receive smaller penalties. Since the

original OW $k$ -means is formulated in a relocation-style update with repeated weight/-centroid updates, we use a computationally streamlined variant that retains the same silhouette-to-weight mapping but computes silhouettes using K-SIL’s centroid-distance proxy (§3.3) and alternates reweighting with  $k$ -means weighted updates. For each dataset, we set the number of clusters  $k$  to the ground-truth number of classes reported in §5.1. We then evaluate each method over 10 independent runs with different random initializations (defaults parameters for each method). For a given run (seed/random state), all methods are initialized from the same set of randomly chosen initial centroids, ensuring a fair comparison and isolating the effect of the update rules from favorable initializations. To assess clustering performance, we compute the silhouette score (SIL), clustering accuracy (ACC), obtained after optimally matching cluster labels to class labels via the Hungarian algorithm, normalized mutual information (NMI), and the adjusted Rand index (ARI). Tab. 1 reports mean values over runs. Full results, including 95% Student- $t$  confidence intervals and mean runtime comparisons in seconds (s), are provided in Appendix C Tab. C1, with additional Adjusted Mutual Information and Davies–Bouldin results in Appendix Tab. C3.

#### **$k$ -means++ initialization.**

We additionally compare K-SIL to  $k$ -means in the  $k$ -means++ seeding regime, reporting the relative change in mean SIL/ARI/NMI over 120 independent random states (Fig. 5). Since  $k$ -means++ substantially improves the quality of the  $k$ -means solution, improvements are expected to be more moderate; nevertheless, K-SIL is favorable on nearly all datasets and the few exceptions are negligible. Overall, improvements occur more often and are typically larger in magnitude than the rare, very small regressions.

#### **Suboptimal $k$ .**

We examine the robustness of K-SIL when the number of clusters is misspecified: for each dataset with ground-truth  $k^*$ , we run K-SIL with  $k \in \{k^* - 5, \dots, k^* + 5\}$  (restricting to  $k \geq 2$  when  $k^* = 2$ ), and repeat each setting over multiple random initializations/seeds to account for stochasticity. We then average the resulting scores across runs and datasets. We report external agreement via ARI and internal structure via the silhouette score (SIL) (Fig. 4; ACC in Appendix Fig. C2).

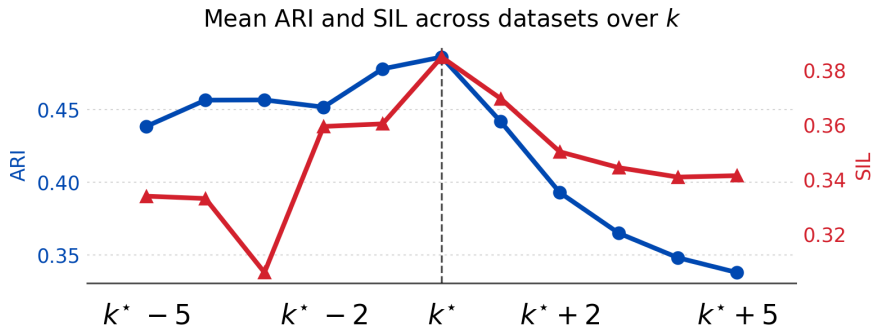


**Fig. 4:** Mean ARI and SIL across multiple random initializations and datasets (§5.1) as a function of the number of clusters  $k \in \{k^* - 5, k^* - 4, \dots, k^*, \dots, k^* + 4, k^* + 5\}$ .

**Table 1:** Mean SIL/ACC/NMI/ARI values of  $k$ -means, LOF $k$ -means, iLOF $k$ -means, OW $k$ -means, and K-SIL over runs (95% Student- $t$  confidence intervals and mean runtime comparisons in seconds in Appendix Tab. C1). Highest mean values in **bold**.

Dataset	Metric	$k$ -means	LOF $k$ -means	iLOF $k$ -means	OW $k$ -means	K-SIL
MIP	SIL	0.564	0.560	0.559	0.556	<b>0.612</b>
	ACC	0.382	0.381	0.388	0.383	<b>0.393</b>
	NMI	0.421	0.420	0.429	0.419	<b>0.444</b>
	ARI	0.223	0.221	0.230	0.222	<b>0.243</b>
WNE	SIL	0.411	0.410	0.418	0.397	<b>0.430</b>
	ACC	0.931	0.941	0.933	0.938	<b>0.972</b>
	NMI	0.839	0.855	0.843	0.835	<b>0.893</b>
	ARI	0.846	0.868	0.854	0.844	<b>0.914</b>
BRC	SIL	0.471	0.467	0.467	0.453	<b>0.492</b>
	ACC	0.908	0.909	0.908	0.907	<b>0.919</b>
	NMI	0.542	0.546	0.542	0.542	<b>0.594</b>
	ARI	0.662	0.666	0.664	0.660	<b>0.700</b>
HTR	SIL	0.684	0.679	0.684	0.653	<b>0.749</b>
	ACC	0.943	0.940	0.943	0.933	<b>0.965</b>
	NMI	0.442	0.423	0.442	0.391	<b>0.572</b>
	ARI	0.635	0.621	0.635	0.590	<b>0.722</b>
VCL	SIL	0.587	0.589	0.588	0.575	<b>0.602</b>
	ACC	0.413	0.418	0.413	0.412	<b>0.428</b>
	NMI	0.163	0.168	0.163	0.168	<b>0.172</b>
	ARI	0.116	0.120	0.117	0.114	<b>0.125</b>
SMS	SIL	0.099	0.099	0.099	0.093	<b>0.111</b>
	ACC	0.845	0.845	0.845	0.834	<b>0.860</b>
	NMI	0.343	0.343	0.343	0.328	<b>0.364</b>
	ARI	0.414	0.414	0.414	0.387	<b>0.452</b>
MDS	SIL	0.338	0.344	0.347	0.326	<b>0.379</b>
	ACC	0.801	0.817	0.793	0.800	<b>0.845</b>
	NMI	0.876	0.886	0.878	0.877	<b>0.894</b>
	ARI	0.767	0.780	0.759	0.768	<b>0.803</b>
INR	SIL	0.563	0.575	0.570	0.548	<b>0.606</b>
	ACC	0.601	0.632	0.600	0.638	<b>0.684</b>
	NMI	0.093	0.094	0.092	0.100	<b>0.104</b>
	ARI	0.051	0.080	0.048	0.089	<b>0.133</b>
DBT	SIL	0.303	0.306	0.302	0.269	<b>0.316</b>
	ACC	0.684	0.684	0.683	0.688	<b>0.699</b>
	NMI	0.082	0.083	0.087	0.091	<b>0.108</b>
	ARI	0.127	0.127	0.127	0.139	<b>0.150</b>
BBC	SIL	0.184	0.182	0.184	0.178	<b>0.188</b>
	ACC	0.886	0.872	0.877	0.876	<b>0.896</b>
	NMI	0.837	0.822	0.833	0.828	<b>0.839</b>
	ARI	0.830	0.810	0.822	0.815	<b>0.837</b>
LKM	SIL	0.204	0.174	0.194	0.198	<b>0.226</b>
	ACC	0.672	0.672	0.674	0.639	<b>0.717</b>
	NMI	0.066	0.111	0.098	0.048	<b>0.123</b>
	ARI	0.097	0.123	0.121	0.064	<b>0.171</b>
RES	SIL	0.242	0.244	0.242	0.224	<b>0.252</b>
	ACC	0.491	0.491	0.482	0.460	<b>0.504</b>
	NMI	0.519	0.522	0.520	0.509	<b>0.527</b>
	ARI	0.349	0.352	0.344	0.320	<b>0.359</b>

Dataset	Metric	$k$ -means	LOF $k$ -means	iLOF $k$ -means	OW $k$ -means	K-SIL
B77	SIL	0.304	0.300	0.304	0.288	<b>0.314</b>
	ACC	0.546	0.542	0.545	0.538	<b>0.553</b>
	NMI	0.734	0.733	<b>0.735</b>	0.732	<b>0.735</b>
	ARI	0.444	0.438	<b>0.446</b>	0.440	<b>0.446</b>
CLC	SIL	0.286	0.288	0.287	0.274	<b>0.294</b>
	ACC	0.687	0.687	0.684	0.677	<b>0.693</b>
	NMI	0.858	0.858	<b>0.859</b>	0.855	<b>0.859</b>
	ARI	0.548	0.548	0.548	0.540	<b>0.552</b>
STL	SIL	0.257	0.264	0.258	0.250	<b>0.265</b>
	ACC	0.843	0.858	0.840	0.832	<b>0.859</b>
	NMI	0.894	0.893	0.894	0.888	<b>0.899</b>
	ARI	0.820	0.829	0.819	0.806	<b>0.836</b>

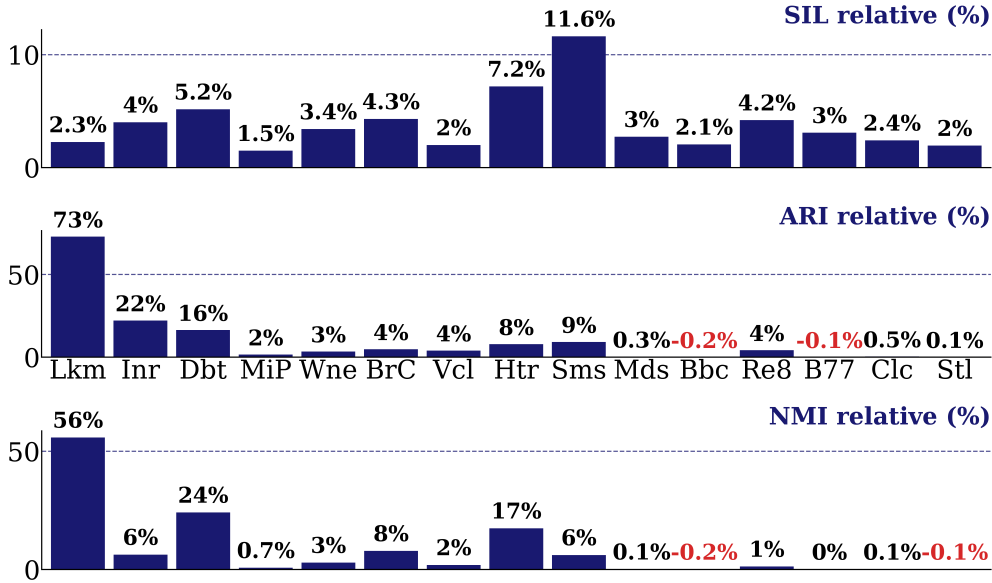
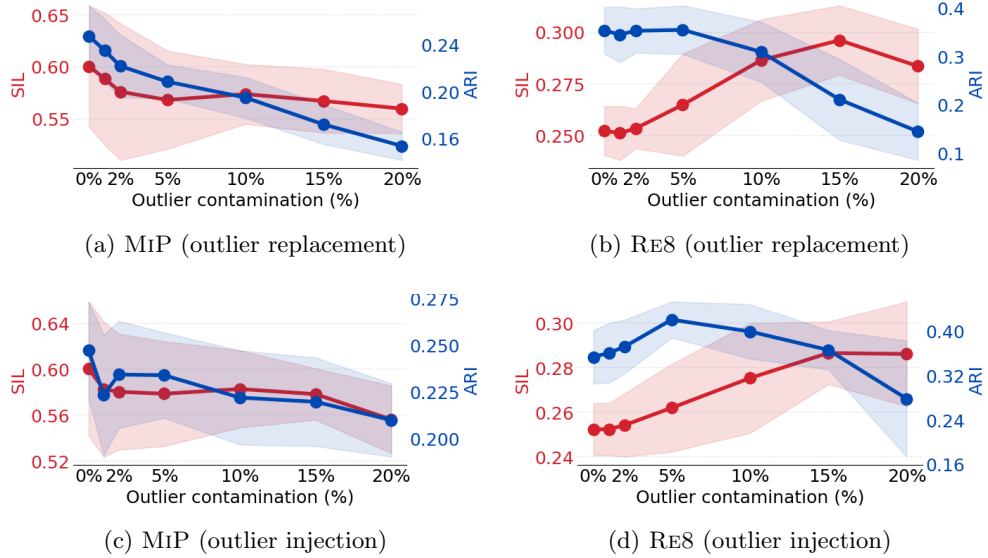


Fig. 5: Mean relative change (%  $\uparrow$   $\downarrow$ ) in SIL, ARI, NMI of K-SIL over  $k$ -means (with  $k$ -means++ initialization) over 120 independent runs across datasets (§5.1).

### Stress tests.

To probe robustness to outlier “contamination,” we stress-test K-SIL on two representative datasets, MiP and RE8. We fix  $k = k^*$  and rerun K-SIL for increasing outlier levels  $\varepsilon \in \{1, 2, 5, 10, 15, 20\}\%$ , averaging over multiple random initializations; for each  $\varepsilon$  we report mean $\pm$ std of SIL and ARI. We consider two protocols: (i) *outlier replacement*, which replaces an  $\varepsilon$  fraction of original points with synthetic outliers (injecting noise while removing informative samples); and (ii) *outlier injection*, which appends  $\varepsilon$  synthetic outliers while keeping all original points. In (ii), ARI is computed on the original points only, directly measuring preservation of the clean-label structure. The resulting trends are summarized in Fig. 6 (6a, 6b: replacement; 6c, 6d: injection).



**Fig. 6:** Stress tests on MiP and RE8. Top row (a), (b): outlier replacement; bottom row (c), (d): outlier injection. Mean **SIL** (left axis) and **ARI** (right axis) vs. outlier contamination over runs %; shaded areas indicate  $\pm$  std over runs.

### Ablations.

We perform ablations to assess the effect of each design choice in K-SiL, modifying one component at a time while keeping the rest unchanged: (a) K-SiL uses weights  $w_i \propto \exp(\tau s_i)$ . We keep the same weighting form but replace the signal  $s_i$  with its building blocks  $a_i, b_i$  (Eq. 7): a-K-SiL replaces  $s_i$  with the intra-cluster term  $a_i$  (using  $1/(a_i + \varepsilon)$ ), emphasizing compactness, while b-K-SiL replaces  $s_i$  with the inter-cluster term  $b_i$ , emphasizing separation (Fig. 7a); (b) we sweep the initial temperature (§3.5)  $\tau_0 \in \{1, 2, 3\}$  (Fig. 7b). An additional ablation over the learning rate  $\eta$  (Eq. 12) is deferred to Appendix Fig. C1.

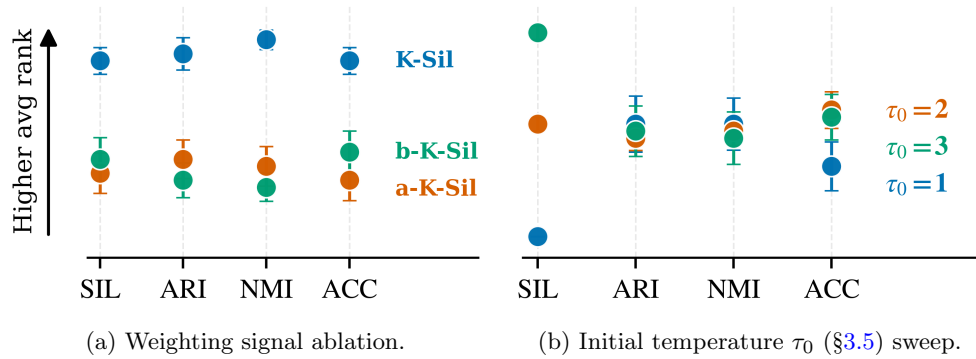


**Fig. 7:** Dots show the average per-dataset rank (higher rank  $\approx$  more frequent method wins) over SIL, ARI, NMI, and ACC; error bars denote SEM across multiple seeds.

### 5.3 Results

K-SIL converges across all datasets and runs. The average centroid movement quickly decays and then plateaus, while the instance-weights become almost perfectly correlated across successive iterations (Fig. 3; Appendix Figs. C3–C6). K-SIL improves internal separation and typically strengthens external agreement. It yields consistent improvements over baselines across datasets and metrics (SIL/ACC/NMI/ARI in Tab. 1 and AMI/DB in Appendix Tab. C3; typically with confidence intervals that are tighter and centered at higher values Appendix Tab. C1). Gains are particularly pronounced on several datasets (e.g., BRC, HTR, WNE, MDS). On more challenging regimes, improvements are naturally more modest, but K-SIL remains stable and competitive, including LKM ( $d \gg n$ ) and large- $k$  benchmarks such as B77 ( $k=77$ ) and CLC ( $k=151$ ). Runtime-wise, K-Sil adds modest overhead versus  $k$ -means, yet is typically faster than iLOF-based reweighting (Appendix Tab. C1). When comparing K-SIL to  $k$ -means in the  $k$ -means++ seeding regime, improvements largely persist despite the stronger baseline (Fig. 5). K-SIL improves on nearly every dataset, and the few declines are tiny (e.g.,  $\approx -0.1\%$  NMI on Bbc and Stl). Across datasets, gains are both more frequent and larger than the rare, minor regressions. Under misspecified cluster counts, SIL and ARI peak around the ground-truth  $k^*$  across datasets (Fig. 4, with the same trend for ACC Appendix Fig. C2), indicating that performance is higher near  $k^*$ , without a systematic bias toward over- or under-clustering. The robustness experiments (Fig. 6) highlight complementary behaviors. Under outlier replacement (Fig. 6a), ARI typically degrades more strongly than SIL, showing that K-SIL can maintain geometric separation even when informative signal is progressively destroyed; on RE8 we also observe silhouette inflation, illustrating that separation-based criteria may become overly optimistic under strong destructive corruption. Under outlier injection (Fig. 6c), K-SIL is markedly more stable, while SIL declines, reflecting that appended outliers do not fit the learned structure. Overall, K-SIL is more reliable under additive contamination, and the tests show that internal separation and label agreement may diverge under replacement noise. The rank-based ablations (Fig. 7a) show that K-SIL ranks best overall, consistently winning against compactness-only ( $a_i$ ) and separation-only ( $b_i$ ) variants across datasets and metrics (SIL/ARI/NMI/ACC), supporting the centroid-margin silhouette proxy as a balanced confidence signal. The initial temperature ablation (Fig. 7b) shows that higher  $\tau_0$  can make the early weighting more selective and may inflate SIL, while improvements in external metrics depend on the degree to which internal geometry aligns with label structure; overall,  $\tau_0=1$  is a safe default for external agreement (our rule for choosing  $\tau_0 \in \{1, 2\}$  is reported in Appendix C.1).

## 6 Conclusion

We introduced K-SIL, a silhouette-driven instance-weighted  $k$ -means variant that uses a centroid-margin silhouette proxy to turn geometric assignment confidence into a per-cluster instance-weighting distribution at each iteration. By updating each centroid as a softmax-weighted mean of its assigned points and calibrating the sharpness

of reweighting through an adaptive temperature guided by a macro-averaged silhouette criterion, K-SIL emphasizes reliable instances and suppresses ambiguous or noisy influence. On the theory side, we established local convergence under standard separation conditions. Empirically, K-SIL consistently improves clustering quality across diverse datasets and remains competitive under strong baselines and stress settings. These results highlight a broadly useful principle for improving centroid-based clustering: use within-iteration geometric signals to steer centroid updates toward reliably assigned structure. Future work includes principled selection or learning of representations and embedding spaces where silhouette-based geometry aligns most strongly with external-label structure, making K-SIL’s weighting most informative.

## Declarations

- Funding: This work was supported by the Archimedes Research Unit, Athena Research Center, through the project “ARCHIMEDES Unit: Research in Artificial Intelligence, Data Science, and Algorithms”, implemented within the framework of the National Recovery and Resilience Plan “Greece 2.0” and funded by the European Union – NextGenerationEU.
- Conflict of interest/Competing interests: ‘Not applicable’
- Ethics approval and consent to participate: ‘Not applicable’
- Consent for publication: ‘Not applicable’
- Data availability: ‘Not applicable’
- Materials availability: ‘Not applicable’
- Code availability: Available at [https://github.com/semoglou/ksil\\_clustering](https://github.com/semoglou/ksil_clustering).
- Author contribution: AS: Methodology; Formal Analysis; Software; Writing (original draft), AL: Methodology; Supervision; Writing (review/editing), JP: Conceptualization; Supervision; Writing (review/editing).

## References

- [1] Jain, A.K., Murty, M.N., Flynn, P.J.: Data clustering: A review. *ACM Computing Surveys* **31**(3), 264–323 (1999)
- [2] Kaufman, L., Rousseeuw, P.J.: *Finding groups in data: An introduction to cluster analysis*. (1990)
- [3] MacQueen, J.B.: Some methods for classification and analysis of multivariate observations. In: *Proceedings of the 5th Berkeley Symposium on Mathematical Statistics and Probability*, pp. 281–297 (1967)
- [4] Ikotun, A.M., Absalom, E.E., Abualigah, L.M., Abuhaija, B., Jia, H.: K-means clustering algorithms: A comprehensive review, variants analysis, and advances in the era of big data. *Inf. Sci.* **622**, 178–210 (2022)
- [5] Bubeck, S., Meila, M., Luxburg, U.: How the initialization affects the stability of the k-means algorithm. *ESAIM: Probability and Statistics* **16** (2009)

- [6] Jain, A.K.: Data clustering: 50 years beyond k-means. *Pattern Recognit. Lett.* **31**, 651–666 (2008)
- [7] Xu, R., Wunsch, D.: Survey of clustering algorithms. *IEEE Transactions on Neural Networks* **16**(3), 645–678 (2005)
- [8] Moggridge, P., Helian, N., Sun, Y., Lilley, M., Veneziano, V.: Instance weighted clustering: Local outlier factor and k-means. In: Iliadis, L., Angelov, P.P., Jayne, C., Pimenidis, E. (eds.) *Proceedings of the 21st EANN (Engineering Applications of Neural Networks) 2020 Conference*, pp. 435–446. Springer, Cham (2020)
- [9] Wang, F., Franco-Penya, H.-H., Kelleher, J.D., Pugh, J., Ross, R.: An analysis of the application of simplified silhouette to the evaluation of k-means clustering validity. In: Perner, P. (ed.) *Machine Learning and Data Mining in Pattern Recognition*, pp. 291–305. Springer, Cham (2017)
- [10] Rousseeuw, P.J.: Silhouettes: A graphical aid to the interpretation and validation of cluster analysis. *Journal of Computational and Applied Mathematics* **20**, 53–65 (1987)
- [11] Dudek, A.: Silhouette index as clustering evaluation tool. In: *Classification and Data Analysis: Theory and Applications* 28, pp. 19–33 (2020). Springer
- [12] Pavlopoulos, J., Vardakas, G., Likas, A.: Revisiting silhouette aggregation. In: *Discovery Science*, pp. 354–368. Springer, Cham (2025)
- [13] Ester, M., Kriegel, H.-P., Sander, J., Xu, X.: A density-based algorithm for discovering clusters in large spatial databases with noise. In: *Proceedings of the 2nd International Conference on Knowledge Discovery and Data Mining (KDD)*, pp. 226–231 (1996)
- [14] Müllner, D.: Modern hierarchical, agglomerative clustering algorithms. *arXiv preprint arXiv:1109.2378* (2011)
- [15] Reynolds, D.A.: Gaussian mixture models. *Encyclopedia of Biometrics*, 659–663 (2009)
- [16] Ng, A.Y., Jordan, M.I., Weiss, Y.: On spectral clustering: Analysis and an algorithm. In: *Advances in Neural Information Processing Systems (NeurIPS)*, vol. 14 (2002)
- [17] Arthur, D., Vassilvitskii, S.: K-means++ the advantages of careful seeding. In: *Proceedings of the Eighteenth Annual ACM-SIAM Symposium on Discrete Algorithms*, pp. 1027–1035 (2007)
- [18] Bachem, O., Lucic, M., Krause, A.: Fast and provably good seedings for k-means. In: *Advances in Neural Information Processing Systems (NeurIPS)*, pp. 55–63

(2016)

- [19] Likas, A., Vlassis, N., Verbeek, J.J.: The global  $k$ -means clustering algorithm. *Pattern recognition* **36**(2), 451–461 (2003)
- [20] Vardakas, G., Likas, A.: Global  $k$ -means++: an effective relaxation of the global  $k$ -means clustering algorithm. *arXiv preprint arXiv:2211.12271* (2022)
- [21] Arbelaitz, O., Gurrutxaga, I., Muguerza, J., Pérez, J.M., Perona, I.: An extensive comparative study of cluster validity indices. *Pattern recognition* **46**(1), 243–256 (2013)
- [22] Bombina, P., Tally, D., Abrams, Z.B., Coombes, K.R.: Sillyputty: Improved clustering by optimizing the silhouette width. *PLOS ONE* **19**(6), 1–17 (2024)
- [23] Batool, F., Hennig, C.: Clustering with the average silhouette width. *Computational Statistics & Data Analysis* **158**, 107190 (2021)
- [24] Huang, J.Z., Ng, M.K., Rong, H., Li, Z.: Automated variable weighting in  $k$ -means type clustering. *IEEE Transactions on Pattern Analysis and Machine Intelligence* **27**(5), 657–668 (2005)
- [25] Jing, L., Ng, M.K., Huang, J.Z.: An entropy weighting  $k$ -means algorithm for subspace clustering of high-dimensional sparse data. *IEEE Transactions on Knowledge and Data Engineering* **19**(8), 1026–1041 (2007)
- [26] Chan, E.Y., Ching, W.K., Ng, M.K., Huang, J.Z.: An optimization algorithm for clustering using weighted dissimilarity measures. *Pattern Recognition* **37**(5), 943–952 (2004)
- [27] Lai, H., Huang, T., Lu, B., Zhang, S., Xiaog, R.: Silhouette coefficient-based weighting  $k$ -means algorithm. *Neural Computing and Applications* **37**, 3061–3075 (2024)
- [28] Moggridge, P., Helian, N., Sun, Y., Lilley, M., Veneziano, V.: Instance weighted clustering: Local outlier factor and  $k$ -means. In: Iliadis, L., Angelov, P.P., Jayne, C., Pimenidis, E. (eds.) *Proceedings of the 21st EANN (Engineering Applications of Neural Networks) 2020 Conference*, pp. 435–446. Springer, Cham (2020)
- [29] Gondeau, A., Aouabed, Z., Hijri, M., Peres-Neto, P., Makarenkov, V.: Object weighting: A new clustering approach to deal with outliers and cluster overlap in computational biology. *IEEE/ACM transactions on computational biology and bioinformatics / IEEE, ACM* **18**, 633–643 (2021)

## Appendix A Theoretical results

### Proof of L.1 (Stability near $\mu_\star$ ).

*Proof* Fix  $j$  and  $x_i$  with  $c_\star(i) = j$ . Then  $\|x_i - \mu_{\star,j}\| \leq r$ . For any  $\mu$  with  $\|\mu - \mu_\star\|_{\infty,2} \leq r$ , we have  $\|\mu_j - \mu_{\star,j}\| \leq \|\mu - \mu_\star\|_{\infty,2} \leq r$ , hence

$$\|x_i - \mu_j\| \leq \|x_i - \mu_{\star,j}\| + \|\mu_j - \mu_{\star,j}\| \leq r + r = 2r.$$

For any other cluster  $\ell \neq j$ ,

$$\|x_i - \mu_\ell\| \geq \|\mu_{\star,\ell} - \mu_{\star,j}\| - \|x_i - \mu_{\star,j}\| - \|\mu_\ell - \mu_{\star,\ell}\| \geq 5r - r - r = 3r.$$

Thus  $\mu_j$  remains the nearest centroid to  $x_i$  for all  $\mu \in U_\mu$ , and therefore  $c(\mu) = c_\star$ . Since  $H_j(\mu, \tau)$  is a convex combination of  $x_i$  for  $i \in C_j = \{i : c_\star(i) = j\}$  and  $\|x_i - \mu_{\star,j}\| \leq r$  for  $i \in C_j$  (A.1), we have  $\|H_j(\mu, \tau) - \mu_{\star,j}\| \leq r \forall j \Rightarrow \|H(\mu, \tau) - \mu_\star\|_{\infty,2} \leq r$  and  $H(\mu, \tau) \in U_\mu$ .  $\square$

### Proof of L.2 (Silhouette Lipschitz bound).

*Proof* Let  $i : c_\star(i) = j$ . By L.1:

$$a_i(\mu) = \|x_i - \mu_j\| \leq 2r, \quad b_i(\mu) = \min_{\ell \neq j} \|x_i - \mu_\ell\| \geq 3r$$

for any  $\mu \in U_\mu$ . Also, by definition,

$$|a_i(\mu) - a_i(\mu')| \leq \|\mu - \mu'\|_{\infty,2}, \quad |b_i(\mu) - b_i(\mu')| \leq \|\mu - \mu'\|_{\infty,2}.$$

Since  $s_i(\mu) = (b_i(\mu) - a_i(\mu))/b_i(\mu) = 1 - a_i(\mu)/b_i(\mu)$  (§3.3) on  $U_\mu$ , we bound the ratio:

$$\left| \frac{a}{b} - \frac{a'}{b'} \right| \leq \frac{|a - a'|}{b} + \frac{a'|b - b'|}{bb'} \leq \frac{1}{3r} \|\mu - \mu'\|_{\infty,2} + \frac{2r}{(3r)^2} \|\mu - \mu'\|_{\infty,2} = \frac{5}{9r} \|\mu - \mu'\|_{\infty,2}.$$

This proves the bound for  $s_i$  (Eq. 5).  $S(\mu)$  (Eq. 6) is an average of the  $s_i(\mu)$  with fixed nonnegative weights (since clusters are fixed on  $U_\mu$ ), so the same Lipschitz constant applies.  $\square$

### Proof of L.3 (Softmax Lipschitz).

*Proof* Write  $f(u) = \text{softmax}(u)$ , so  $f : \mathbb{R}^m \rightarrow \mathbb{R}^m$  is a vector-valued map. Fix  $z \in \mathbb{R}^m$  and set

$$p = f(z) = (p_1, \dots, p_m), \quad \text{i.e. } p_i = \exp(z_i) / \sum_{\ell=1}^m \exp(z_\ell)$$

The derivative of  $f$  at  $z$  is its Jacobian matrix  $J(z) \in \mathbb{R}^{m \times m}$  with entries  $J_{i\ell}(z) = \partial p_i / \partial z_\ell$ . A direct computation gives the standard identity  $J_{i\ell}(z) = p_i(\delta_{i\ell} - p_\ell)$ , which in matrix form is  $J(z) = \text{diag}(p) - pp^\top$ , where  $\text{diag}(p)$  is the diagonal matrix with diagonal  $(p_1, \dots, p_m)$  and  $(pp^\top)_{i\ell} = p_i p_\ell$ . To bound the operator norm  $\|J(z)\|_{\infty \rightarrow 1}$ , let  $v \in \mathbb{R}^m$  with  $\|v\|_\infty \leq 1$ . Define the  $p$ -weighted average  $\mu = \langle p, v \rangle = \sum_{i=1}^m p_i v_i$ . Using  $J(z) = \text{diag}(p) - pp^\top$  we obtain, for each coordinate  $i$ ,

$$(J(z)v)_i = p_i v_i - p_i \sum_{\ell=1}^m p_\ell v_\ell = p_i(v_i - \mu).$$

Hence  $\|J(z)v\|_1 = \sum_{i=1}^m |(J(z)v)_i| = \sum_{i=1}^m p_i |v_i - \mu|$ . We now maximize this quantity over the cube  $\{v : \|v\|_\infty \leq 1\}$ . The map  $v \mapsto \sum_i p_i |v_i - \langle p, v \rangle|$  is convex in  $v$  (absolute value is convex and  $\langle p, v \rangle$  is linear), so its maximum over a compact convex set is attained at an extreme point of the set; here the extreme points are exactly the sign vectors  $v \in \{\pm 1\}^m$ .

Fix such a  $v \in \{\pm 1\}^m$  and write  $p_+ = \sum_{i:v_i=1} p_i$  and  $p_- = \sum_{i:v_i=-1} p_i = 1 - p_+$ . Then the weighted average is  $\mu = \langle p, v \rangle = p_+ - p_- = 2p_+ - 1$ . Moreover, for indices with  $v_i = 1$  we have  $|v_i - \mu| = |1 - \mu|$ , and for  $v_i = -1$  we have  $|v_i - \mu| = |-1 - \mu|$ , so

$$\sum_{i=1}^m p_i |v_i - \mu| = p_+ |1 - \mu| + p_- |-1 - \mu| = p_+ \cdot 2(1 - p_+) + p_- \cdot 2p_+ = 4p_+ p_- \leq 1,$$

since  $p_+ p_- \leq \frac{1}{4}$ . Therefore  $\|J(z)v\|_1 \leq 1$  for all  $\|v\|_\infty \leq 1$ , i.e.  $\|J(z)\|_{\infty \rightarrow 1} \leq 1$  for all  $z$ . Finally, apply the mean value theorem for vector-valued functions along the line segment from  $u'$  to  $u$  and taking  $\ell_1$  norms and using the operator-norm bound gives:

$$\begin{aligned} f(u) - f(u') &= \int_0^1 J(u' + t(u - u'))(u - u') dt. \\ \|f(u) - f(u')\|_1 &\leq \int_0^1 \|J(u' + t(u - u'))\|_{\infty \rightarrow 1} dt \|u - u'\|_\infty \leq \|u - u'\|_\infty, \end{aligned}$$

□

#### Proof of L.4 (Lipschitz bounds for the centroid map $H$ ).

*Proof* Fix a cluster  $j$ . Since  $\mu, \mu' \in U_\mu$ , Lemma L.1 implies the labels are constant on  $U_\mu$ , hence  $C_j(\mu) = C_j(\mu') =: C_j$ . Write the weighted update as

$$H_j(\mu, \tau) = \sum_{i \in C_j} p_i(\mu, \tau) x_i, \quad p(\mu, \tau) = \text{softmax}\left(\tau [s_i(\mu)]_{i \in C_j}\right),$$

so that  $\sum_{i \in C_j} p_i(\mu, \tau) = 1$ .

(i) Lipschitz in  $\mu$  (fixed  $\tau$ ). Using  $\sum_{i \in C_j} (p_i(\mu, \tau) - p_i(\mu', \tau)) = 0$  and centering at  $\mu_{\star, j}$ ,

$$H_j(\mu, \tau) - H_j(\mu', \tau) = \sum_{i \in C_j} (p_i(\mu, \tau) - p_i(\mu', \tau)) (x_i - \mu_{\star, j}).$$

By A.1,  $\|x_i - \mu_{\star, j}\| \leq r$  for all  $i \in C_j$ , hence

$$\|H_j(\mu, \tau) - H_j(\mu', \tau)\| \leq \sum_{i \in C_j} |p_i(\mu, \tau) - p_i(\mu', \tau)| \|x_i - \mu_{\star, j}\| \leq r \|p(\mu, \tau) - p(\mu', \tau)\|_1.$$

Let  $u(\mu) = \tau [s_i(\mu)]_{i \in C_j}$  be the logits. Lemma L.3 gives

$$\|p(\mu, \tau) - p(\mu', \tau)\|_1 \leq \|u(\mu) - u(\mu')\|_\infty \leq \tau \max_{i \in C_j} |s_i(\mu) - s_i(\mu')|.$$

Applying Lemma L.2 yields  $\max_{i \in C_j} |s_i(\mu) - s_i(\mu')| \leq \frac{5}{9r} \|\mu - \mu'\|_{\infty, 2}$ , so

$$\|H_j(\mu, \tau) - H_j(\mu', \tau)\| \leq r \cdot \tau \cdot \frac{5}{9r} \|\mu - \mu'\|_{\infty, 2} = \frac{5\tau}{9} \|\mu - \mu'\|_{\infty, 2}.$$

Taking  $\max_{1 \leq j \leq k}$  gives the first claim:  $\|H(\mu, \tau) - H(\mu', \tau)\|_{\infty, 2} \leq \frac{5\tau}{9} \|\mu - \mu'\|_{\infty, 2}$ .

(ii) Lipschitz in  $\tau$  (fixed  $\mu$ ). Fix  $\mu$  and consider

$$H_j(\mu, \tau) - H_j(\mu, \tau') = \sum_{i \in C_j} (p_i(\mu, \tau) - p_i(\mu, \tau')) (x_i - \mu_{\star, j}),$$

hence  $\|H_j(\mu, \tau) - H_j(\mu, \tau')\| \leq r \|p(\mu, \tau) - p(\mu, \tau')\|_1$  as above. With logits  $u = \tau [s_i(\mu)]_{i \in C_j}$  and  $u' = \tau' [s_i(\mu)]_{i \in C_j}$ , Lemma L.3 gives

$$\|p(\mu, \tau) - p(\mu, \tau')\|_1 \leq \|u - u'\|_\infty = |\tau - \tau'| \| [s_i(\mu)]_{i \in C_j} \|_\infty \leq |\tau - \tau'|,$$

since  $s_i(\mu) \in [0, 1]$ . Therefore

$$\|H_j(\mu, \tau) - H_j(\mu, \tau')\| \leq r|\tau - \tau'|,$$

and taking  $\max_j$  gives

$$\|H(\mu, \tau) - H(\mu, \tau')\|_{\infty, 2} \leq r|\tau - \tau'|.$$

□

### Proof of Theorem (Local convergence under bounded temperature).

*Proof* (i) Invariance and fixed labels.

Since  $\mu_0 \in U_\mu$ , Lemma L.1 gives  $c(\mu_0) = c_\star$  and  $\mu_1 = H(\mu_0, \tau_1) \in U_\mu$ .

Repeating the same argument inductively yields  $\mu_t \in U_\mu$  and  $c(\mu_t) = c_\star$  for all  $t$ .

In particular, the index sets  $C_j(\mu_t)$  (hence the sizes  $n_j(\mu_t)$  and the bound  $\tau_{\max}(t)$ ) are constant on  $U_\mu$ .

(ii) One-step contraction for the centroid increments.

Using  $\mu_{t+1} = H(\mu_t, \tau_{t+1})$  and  $\mu_t = H(\mu_{t-1}, \tau_t)$ ,

$$H(\mu_t, \tau_{t+1}) - H(\mu_{t-1}, \tau_t) = \underbrace{[H(\mu_t, \tau_{t+1}) - H(\mu_{t-1}, \tau_{t+1})]}_{(A)} + \underbrace{[H(\mu_{t-1}, \tau_{t+1}) - H(\mu_{t-1}, \tau_t)]}_{(B)}.$$

By Lemma L.4 and  $\tau_{t+1} \leq \bar{\tau}$  (A.2(i)):

$$\|(A)\|_{\infty, 2} \leq \frac{5\tau_{t+1}}{9} \|\mu_t - \mu_{t-1}\|_{\infty, 2} \leq \frac{5\bar{\tau}}{9} d_t.$$

Also by Lemma L.4,

$$\|(B)\|_{\infty, 2} \leq r|\tau_{t+1} - \tau_t|.$$

We write the raw multiplicative update (Eq. 12) as  $\tau_{t+1}^{\text{raw}} = \tau_t \exp\{\eta R(S_t, S_{t-1})\}$ , and recall  $\tau_{t+1} = \text{clip}_{[\tau_{\min}, \tau_{\max}(t)]}(\tau_{t+1}^{\text{raw}})$  (Eq. 13).

Since  $\tau_t \in [\tau_{\min}, \tau_{\max}(t)]$  (A.2(i)), lower clipping is non-expansive, so

$$|\tau_{t+1} - \tau_t| \leq |\tau_{t+1}^{\text{raw}} - \tau_t| = \tau_t |\exp\{\eta R(S_t, S_{t-1})\} - 1|.$$

Using convexity of  $r \mapsto e^{\eta r}$  on  $[-1, 1]$ , for all  $|r| \leq 1$  we have  $|e^{\eta r} - 1| \leq (e^\eta - 1)|r|$ .

Since  $|R(S_t, S_{t-1})| \leq 1$ , it follows that

$$|\tau_{t+1} - \tau_t| \leq \bar{\tau}(e^\eta - 1)|R(S_t, S_{t-1})|.$$

Under A.2(ii)–(iii),  $R(S_t, S_{t-1}) = \tilde{r}(S_t, S_{t-1})$ , hence

$$|R(S_t, S_{t-1})| = \frac{|S_t - S_{t-1}|}{1 - S_{t-1} + \epsilon} \leq \frac{1}{\alpha} |S(\mu_t) - S(\mu_{t-1})| \leq \frac{L_s}{\alpha} d_t,$$

where we used Lemma L.2. Combining the bounds and  $L_s = \frac{5}{9\bar{r}}$  gives

$$d_{t+1} \leq \left[ \frac{5\bar{\tau}}{9} + r\bar{\tau}(e^\eta - 1)\frac{L_s}{\alpha} \right] d_t = \frac{5\bar{\tau}}{9} \left( 1 + \frac{e^\eta - 1}{\alpha} \right) d_t = \bar{q} d_t.$$

Since,  $\bar{q} = \frac{5\bar{\tau}}{9} \left( 1 + \frac{e^\eta - 1}{\alpha} \right) < 1$ , proving (ii).

(iii) Convergence of  $\mu_t$ ,  $S_t$ , and  $\tau_t$ . From (ii),  $d_t \leq \bar{q}^{t-1} d_1$ , hence  $\sum_{t \geq 1} d_t < \infty$  and  $(\mu_t)$  is Cauchy in  $\|\cdot\|_{\infty, 2}$ . Since  $U_\mu$  is closed,  $\mu_t \rightarrow \mu_\infty \in U_\mu$ . By continuity of  $S(\mu)$  on  $U_\mu$  (labels fixed by (i)), we have  $S_t = S(\mu_t) \rightarrow S(\mu_\infty) = S_\infty$ .

For the temperature, the bound above yields  $|\tau_{t+1} - \tau_t| \leq \bar{\tau}(e^\eta - 1)\frac{L_s}{\alpha} d_t$ , and the right-hand side is summable since  $\sum_t d_t < \infty$ . Thus  $\sum_t |\tau_{t+1} - \tau_t| < \infty$ , so  $(\tau_t)$  is Cauchy and  $\tau_t \rightarrow \tau_\infty \in [\tau_{\min}, \bar{\tau}]$ . Moreover, by continuity of  $H$  and  $\Psi_\eta$  on  $U_\mu \times [0, \bar{\tau}]$  (labels fixed by (i)), the limits satisfy  $\mu_\infty = H(\mu_\infty, \tau_\infty)$  and  $\tau_\infty = \Psi_\eta(\tau_\infty, S_\infty, S_\infty)$ .

□

## Appendix B Empty-cluster re-initialization strategy

After the nearest-centroid reassignment (Eq. 3) at iteration  $t + 1$ , define the index set and size of cluster  $j$  as  $C_j(\mu_{t+1}) = \{i : c(\mu_{t+1})(i) = j\}$ ,  $n_j(\mu_{t+1}) = |C_j(\mu_{t+1})|$ . If a cluster becomes empty, i.e.  $n_j(\mu_{t+1}) = 0$ , we re-initialize its centroid by selecting a point from the currently largest cluster (by size) that lies farthest from that cluster’s centroid. Formally, let  $j_{\max} \in \arg \max_{\ell \in \{1, \dots, k\}} n_\ell(\mu_{t+1})$  denote an index of a largest cluster, and let  $i^* \in \arg \max_{i \in C_{j_{\max}}(\mu_{t+1})} \|x_i - \mu_{t+1, j_{\max}}\|$  be the index of the point farthest from its centroid within that largest cluster. We then re-seed the empty cluster by setting  $\mu_{t+1, j} \leftarrow x_{i^*}$  for each  $j$  such that  $n_j(\mu_{t+1}) = 0$ . Optionally (and in our implementation), we also assign this point to the re-initialized cluster,  $c(\mu_{t+1})(i^*) \leftarrow j$ , to ensure the cluster is non-empty immediately. In addition to truly empty clusters, our implementation applies the *same* re-initialization rule to clusters that are *too small*, i.e. those satisfying  $n_j(\mu_{t+1}) < 3$ . This is a safeguard introduced to maintain the standing assumption used in §3.5 that cluster sizes remain at least three,  $n_j(\mu_t) \geq 3$  for all  $j, t$ : when a cluster has size 1 or 2, its per-cluster silhouette aggregation (Eq. 6) and the temperature dynamics driven by it can become overly noisy and unrepresentative. Thus, whenever  $n_j(\mu_{t+1}) < 3$  occurs, we treat the cluster as effectively empty and re-seed it using the procedure above. This strategy is based on the intuition that points farthest from the dominant cluster’s center are likely to represent under-modeled structure or outlying regions; re-seeding at such a point helps restore the intended number of clusters while exploring uncovered regions. In all experiments reported in §5, no cluster became empty and no cluster satisfied  $n_j(\mu_t) < 3$  at any iteration; the above procedure is included purely as a safeguard.

## Appendix C Empirical Results

**Table C1:** Mean SIL/ACC/NMI/ARI values with 95%  $t$ -confidence intervals, along with mean runtime in seconds (s) per dataset over runs. Gray ranges (---) show confidence intervals; highest mean values are in **bold**.

All experiments were run in a cloud-hosted notebook with 51 GB RAM.

Dataset	Metric	$k$ -means	LOF $k$ -means	iLOF $k$ -means	OW $k$ -means	K-SIL
MIP	SIL	0.564 0.539–0.589	0.560 0.534–0.585	0.559 0.533–0.586	0.556 0.531–0.581	<b>0.612</b> 0.593–0.631
	ACC	0.382 0.373–0.390	0.381 0.370–0.392	0.388 0.377–0.398	0.383 0.374–0.391	<b>0.393</b> 0.385–0.400
	NMI	0.421 0.409–0.433	0.420 0.406–0.433	0.429 0.419–0.440	0.419 0.406–0.432	<b>0.444</b> 0.434–0.454
	ARI	0.223 0.211–0.234	0.221 0.209–0.232	0.230 0.218–0.241	0.222 0.209–0.234	<b>0.243</b> 0.232–0.254
	Runtime (s)	0.002	0.006	0.064	0.020	0.042
	SIL	0.411 0.402–0.420	0.410 0.394–0.427	0.418 0.409–0.427	0.397 0.389–0.406	<b>0.430</b> 0.430–0.430
WNE	ACC	0.931 0.885–0.978	0.941 0.899–0.983	0.933 0.886–0.981	0.938 0.901–0.973	<b>0.972</b> 0.972–0.973

Dataset	Metric	<i>k</i> -means	LOF <i>k</i> -means	iLOF <i>k</i> -means	OW <i>k</i> -means	K-SIL
BRC	NMI	0.839 0.791–0.886	0.855 0.809–0.900	0.843 0.796–0.890	0.835 0.800–0.870	<b>0.893</b> 0.891–0.894
	ARI	0.846 0.784–0.909	0.868 0.811–0.926	0.854 0.792–0.916	0.844 0.798–0.889	<b>0.914</b> 0.913–0.916
	Runtime (s)	0.001	0.003	0.023	0.013	0.018
	SIL	0.471 0.470–0.472	0.467 0.466–0.467	0.467 0.467–0.467	0.453 0.453–0.454	<b>0.492</b> 0.492–0.493
	ACC	0.908 0.905–0.910	0.909 0.908–0.910	0.908 0.907–0.909	0.907 0.905–0.910	<b>0.919</b> 0.919–0.919
	NMI	0.542 0.533–0.552	0.546 0.542–0.549	0.542 0.540–0.544	0.542 0.531–0.552	<b>0.594</b> 0.594–0.594
	ARI	0.662 0.654–0.669	0.666 0.664–0.669	0.664 0.661–0.666	0.660 0.652–0.669	<b>0.700</b> 0.700–0.700
	Runtime (s)	0.002	0.004	0.022	0.016	0.021
	SIL	0.684 0.667–0.701	0.679 0.666–0.691	0.684 0.667–0.701	0.653 0.653–0.654	<b>0.749</b> 0.749–0.750
	ACC	0.943 0.933–0.952	0.940 0.933–0.947	0.943 0.934–0.952	0.933 0.931–0.934	<b>0.965</b> 0.965–0.965
NMI	0.442 0.387–0.497	0.423 0.382–0.465	0.442 0.387–0.497	0.391 0.386–0.395	<b>0.572</b> 0.571–0.573	
ARI	0.635 0.593–0.677	0.621 0.589–0.652	0.635 0.593–0.676	0.590 0.585–0.595	<b>0.722</b> 0.721–0.723	
Runtime (s)	0.006	0.261	6.251	0.072	0.151	
VCL	SIL	0.587 0.555–0.618	0.589 0.560–0.619	0.588 0.557–0.619	0.575 0.547–0.603	<b>0.602</b> 0.572–0.632
	ACC	0.413 0.397–0.428	0.418 0.402–0.434	0.413 0.398–0.429	0.412 0.399–0.425	<b>0.428</b> 0.414–0.442
	NMI	0.163 0.150–0.176	0.168 0.154–0.183	0.163 0.150–0.177	0.168 0.156–0.179	<b>0.172</b> 0.158–0.185
	ARI	0.116 0.109–0.124	0.120 0.112–0.128	0.117 0.109–0.124	0.114 0.105–0.123	<b>0.125</b> 0.118–0.132
	Runtime (s)	0.002	0.006	0.058	0.018	0.024
	SIL	0.099 0.099–0.099	0.099 0.099–0.099	0.099 0.099–0.099	0.093 0.093–0.093	<b>0.111</b> 0.111–0.111
ACC	0.845 0.845–0.845	0.845 0.845–0.845	0.845 0.845–0.845	0.834 0.833–0.834	<b>0.860</b> 0.860–0.860	
NMI	0.343 0.343–0.343	0.343 0.343–0.343	0.343 0.343–0.343	0.328 0.327–0.329	<b>0.364</b> 0.364–0.364	
ARI	0.414 0.414–0.414	0.414 0.414–0.414	0.414 0.414–0.414	0.387 0.385–0.389	<b>0.452</b> 0.452–0.452	
Runtime (s)	0.011	0.105	0.963	0.079	0.107	
MDS	SIL	0.338 0.328–0.348	0.344 0.336–0.351	0.347 0.336–0.357	0.326 0.316–0.336	<b>0.379</b> 0.371–0.387
	ACC	0.801 0.775–0.826	0.817 0.797–0.837	0.793 0.763–0.822	0.800 0.772–0.827	<b>0.845</b> 0.815–0.874
	NMI	0.876 0.864–0.887	0.886 0.877–0.895	0.878 0.867–0.889	0.877 0.864–0.889	<b>0.894</b> 0.882–0.906
	ARI	0.767 0.741–0.792	0.780 0.758–0.801	0.759 0.733–0.785	0.768 0.741–0.796	<b>0.803</b> 0.775–0.832
	Runtime (s)	0.003	0.006	0.088	0.022	0.046
	SIL	0.563 0.543–0.584	0.575 0.556–0.594	0.570 0.554–0.586	0.548 0.534–0.563	<b>0.606</b> 0.606–0.606
ACC	0.601 0.539–0.664	0.632 0.576–0.688	0.600 0.538–0.661	0.638 0.579–0.698	<b>0.684</b> 0.684–0.684	
INR						

Dataset	Metric	<i>k</i> -means	LOF <i>k</i> -means	iLOF <i>k</i> -means	OW <i>k</i> -means	K-SiL
DBT	NMI	<b>0.093</b> 0.088–0.099	<b>0.094</b> 0.090–0.099	<b>0.092</b> 0.087–0.097	<b>0.100</b> 0.095–0.104	<b>0.104</b> 0.104–0.104
	ARI	<b>0.051</b> 0.000–0.113	<b>0.080</b> 0.025–0.136	<b>0.048</b> 0.000–0.109	<b>0.089</b> 0.0029–0.149	<b>0.133</b> 0.133–0.133
	Runtime (s)	<b>0.002</b>	<b>0.003</b>	<b>0.017</b>	<b>0.018</b>	<b>0.018</b>
	SIL	<b>0.303</b> 0.262–0.345	<b>0.306</b> 0.262–0.350	<b>0.302</b> 0.259–0.346	<b>0.269</b> 0.262–0.276	<b>0.316</b> 0.277–0.356
	ACC	<b>0.684</b> 0.666–0.702	<b>0.684</b> 0.666–0.702	<b>0.683</b> 0.666–0.701	<b>0.688</b> 0.671–0.704	<b>0.699</b> 0.683–0.714
	NMI	<b>0.082</b> 0.053–0.112	<b>0.083</b> 0.054–0.111	<b>0.087</b> 0.058–0.116	<b>0.091</b> 0.067–0.115	<b>0.108</b> 0.077–0.138
	ARI	<b>0.127</b> 0.089–0.165	<b>0.127</b> 0.090–0.164	<b>0.127</b> 0.090–0.163	<b>0.139</b> 0.112–0.165	<b>0.150</b> 0.113–0.188
BBC	Runtime (s)	<b>0.002</b>	<b>0.009</b>	<b>0.111</b>	<b>0.018</b>	<b>0.043</b>
	SIL	<b>0.184</b> 0.180–0.187	<b>0.182</b> 0.177–0.186	<b>0.184</b> 0.180–0.188	<b>0.178</b> 0.174–0.182	<b>0.188</b> 0.185–0.191
	ACC	<b>0.886</b> 0.837–0.935	<b>0.872</b> 0.821–0.923	<b>0.877</b> 0.827–0.927	<b>0.876</b> 0.827–0.925	<b>0.896</b> 0.850–0.942
	NMI	<b>0.837</b> 0.811–0.862	<b>0.822</b> 0.790–0.854	<b>0.833</b> 0.807–0.859	<b>0.828</b> 0.799–0.856	<b>0.839</b> 0.816–0.863
	ARI	<b>0.830</b> 0.781–0.879	<b>0.810</b> 0.756–0.864	<b>0.822</b> 0.771–0.872	<b>0.815</b> 0.763–0.866	<b>0.837</b> 0.791–0.884
	Runtime (s)	<b>0.003</b>	<b>0.020</b>	<b>0.159</b>	<b>0.025</b>	<b>0.043</b>
LKM	SIL	<b>0.204</b> 0.163–0.246	<b>0.174</b> 0.142–0.206	<b>0.194</b> 0.147–0.240	<b>0.198</b> 0.158–0.238	<b>0.226</b> 0.150–0.302
	ACC	<b>0.672</b> 0.647–0.698	<b>0.672</b> 0.615–0.729	<b>0.674</b> 0.614–0.733	<b>0.639</b> 0.589–0.689	<b>0.717</b> 0.692–0.742
	NMI	<b>0.066</b> 0.034–0.097	<b>0.111</b> 0.060–0.162	<b>0.098</b> 0.046–0.151	<b>0.048</b> 0.018–0.079	<b>0.123</b> 0.095–0.152
	ARI	<b>0.097</b> 0.055–0.140	<b>0.123</b> 0.048–0.197	<b>0.121</b> 0.036–0.205	<b>0.064</b> 0.010–0.118	<b>0.171</b> 0.121–0.222
	Runtime (s)	<b>0.010</b>	<b>0.019</b>	<b>0.081</b>	<b>0.067</b>	<b>0.096</b>
	RE8	SIL	<b>0.242</b> 0.234–0.250	<b>0.244</b> 0.237–0.251	<b>0.242</b> 0.235–0.250	<b>0.224</b> 0.215–0.233
ACC		<b>0.491</b> 0.441–0.540	<b>0.491</b> 0.466–0.516	<b>0.482</b> 0.448–0.516	<b>0.460</b> 0.419–0.501	<b>0.504</b> 0.458–0.550
NMI		<b>0.519</b> 0.498–0.539	<b>0.522</b> 0.503–0.542	<b>0.520</b> 0.499–0.540	<b>0.509</b> 0.483–0.535	<b>0.527</b> 0.506–0.548
ARI		<b>0.349</b> 0.313–0.385	<b>0.352</b> 0.331–0.373	<b>0.344</b> 0.315–0.373	<b>0.320</b> 0.283–0.358	<b>0.359</b> 0.326–0.392
Runtime (s)		<b>0.008</b>	<b>0.049</b>	<b>0.845</b>	<b>0.042</b>	<b>0.143</b>
B77		SIL	<b>0.304</b> 0.299–0.309	<b>0.300</b> 0.297–0.303	<b>0.304</b> 0.298–0.309	<b>0.288</b> 0.282–0.294
	ACC	<b>0.546</b> 0.535–0.556	<b>0.542</b> 0.534–0.550	<b>0.545</b> 0.534–0.557	<b>0.538</b> 0.525–0.551	<b>0.553</b> 0.542–0.563
	NMI	<b>0.734</b> 0.730–0.739	<b>0.733</b> 0.731–0.735	<b>0.735</b> 0.731–0.739	<b>0.732</b> 0.728–0.736	<b>0.735</b> 0.731–0.739
	ARI	<b>0.444</b> 0.435–0.452	<b>0.438</b> 0.430–0.446	<b>0.446</b> 0.436–0.455	<b>0.440</b> 0.431–0.449	<b>0.446</b> 0.438–0.454
	Runtime (s)	<b>0.057</b>	<b>0.220</b>	<b>3.190</b>	<b>0.656</b>	<b>2.248</b>
	CLC	SIL	<b>0.286</b> 0.284–0.287	<b>0.288</b> 0.286–0.289	<b>0.287</b> 0.286–0.289	<b>0.274</b> 0.273–0.276
ACC		<b>0.687</b> 0.682–0.693	<b>0.687</b> 0.680–0.694	<b>0.684</b> 0.679–0.689	<b>0.677</b> 0.671–0.682	<b>0.693</b> 0.687–0.698

Dataset	Metric	$k$ -means	LOF $k$ -means	iLOF $k$ -means	OW $k$ -means	K-SIL
STL	NMI	0.858	0.858	<b>0.859</b>	0.855	<b>0.859</b>
		0.857–0.860	0.857–0.859	0.858–0.860	0.853–0.856	0.858–0.860
	ARI	0.548	0.548	0.548	0.540	<b>0.552</b>
		0.545–0.552	0.544–0.552	0.545–0.551	0.536–0.543	0.549–0.555
	Runtime (s)	0.248	1.019	6.209	1.282	4.247
	SIL	0.257	0.264	0.258	0.250	<b>0.265</b>
		0.245–0.268	0.255–0.273	0.247–0.270	0.238–0.262	0.254–0.276
	ACC	0.843	0.858	0.840	0.832	<b>0.859</b>
		0.763–0.922	0.794–0.921	0.760–0.921	0.754–0.909	0.789–0.930
	NMI	0.894	0.893	0.894	0.888	<b>0.899</b>
		0.863–0.926	0.869–0.918	0.862–0.925	0.858–0.917	0.872–0.925
	ARI	0.820	0.829	0.819	0.806	<b>0.836</b>
		0.741–0.900	0.771–0.887	0.739–0.899	0.730–0.882	0.767–0.904
	Runtime (s)	0.083	0.493	2.335	0.613	1.244

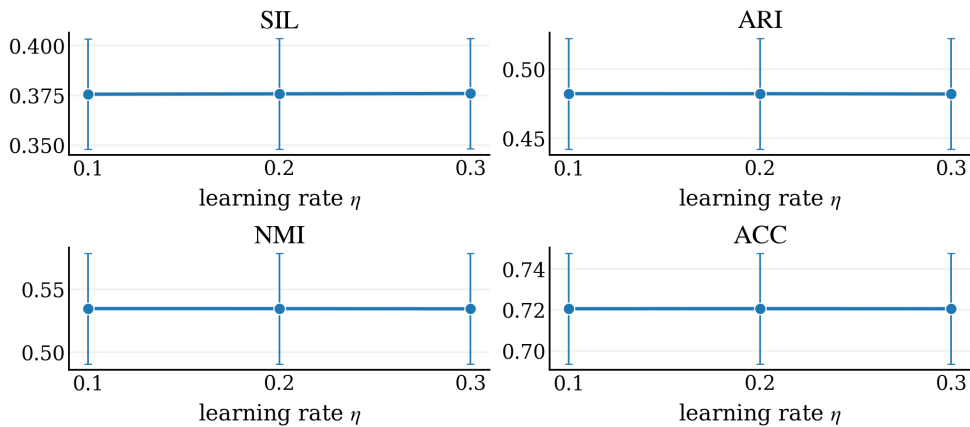


**Fig. C1: Learning-rate ablation.** We examine sensitivity of K-SIL to the learning rate  $\eta$  used in the multiplicative update of the temperature parameter that converts silhouette signals into sample weights (Eq. 12,13). For each dataset, we fix  $k$  to the ground-truth number of classes  $k^*$  (§5.1) and run K-SIL with random initialization for each tested  $\eta \in \{0.1, 0.2, 0.3\}$  over multiple random seeds; we report the mean performance with error bars summarizing variability across runs and datasets. Across all four criteria (SIL, ARI, NMI, and clustering accuracy ACC), performance is essentially flat within the error bars over the tested range, indicating that given the temperature bounds presented in §3.5, the adaptive-temperature mechanism is stable and does not require careful tuning of  $\eta$  (we therefore use a single default value  $\eta = 0.2$  in the main experiments in §5).

**Table C2:** Exact vs. centroid-based approximate silhouette scores computed on a reference  $k$ -means run for each dataset. “Exact” denotes `sklearn.metrics.silhouette_samples` (pairwise point distances), while “Approx” denotes our centroid-margin proxy. Pearson correlation and mean absolute error (MAE) are computed between per-point exact and approximate silhouette values. Reported times are seconds for computing per-point silhouette scores; Speedup is the ratio  $\text{Time}_{\text{Exact}}/\text{Time}_{\text{Approx}}$ .

Dataset	Pearson	MAE	Time Exact (s)	Time Approx (s)	Speedup
LKM	0.738	0.088	0.0110	0.0022	4.8x
INR	0.951	0.103	0.0090	0.0006	15.0x
DBT	0.938	0.118	0.0140	0.0006	23.2x
MIP	0.924	0.105	0.0240	0.0009	27.7x
WNE	0.925	0.134	0.0020	0.0004	3.9x
BRC	0.850	0.136	0.0110	0.0007	17.2x
VCL	0.926	0.098	0.0190	0.0007	27.6x
HTR	0.894	0.088	2.6680	0.0022	1219.6x
SMS	0.849	0.056	0.3380	0.0019	177.0x
MDS	0.964	0.124	0.0070	0.0007	9.9x
BBC	0.935	0.077	0.0550	0.0011	48.7x
RE8	0.947	0.094	0.1980	0.0014	138.5x
B77	0.928	0.116	1.2460	0.0136	91.5x
CLC	0.925	0.115	4.3530	0.0279	156.0x
STL	0.946	0.103	1.1570	0.0074	156.3x

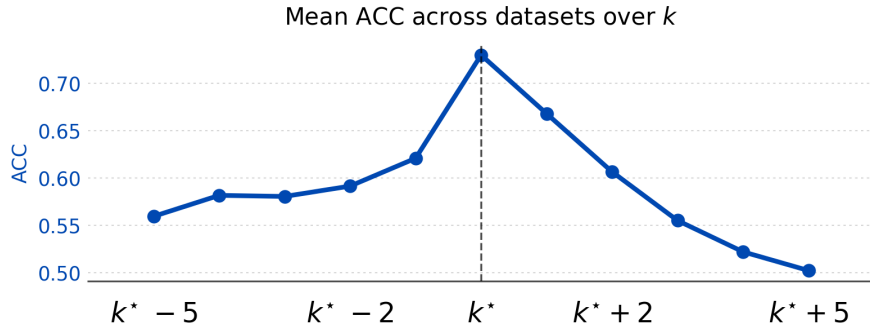
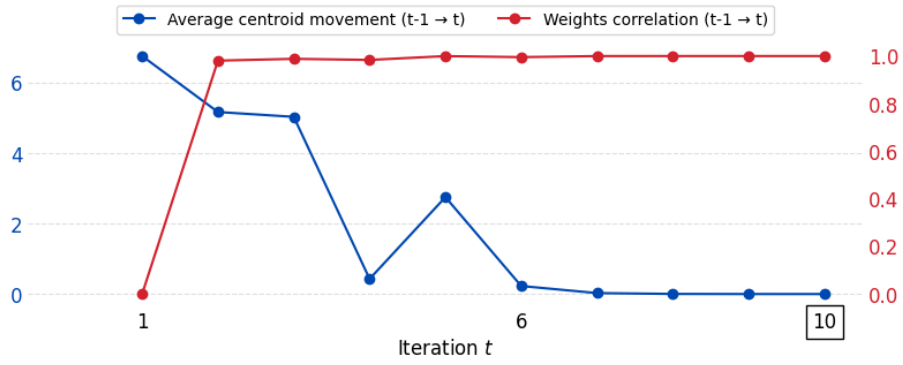


**Fig. C2:** Mean ACC across multiple random initializations and datasets (§5.1) as a function of the number of clusters  $k \in \{k^* - 5, k^* - 4, \dots, k^*, \dots, k^* + 4, k^* + 5\}$ .

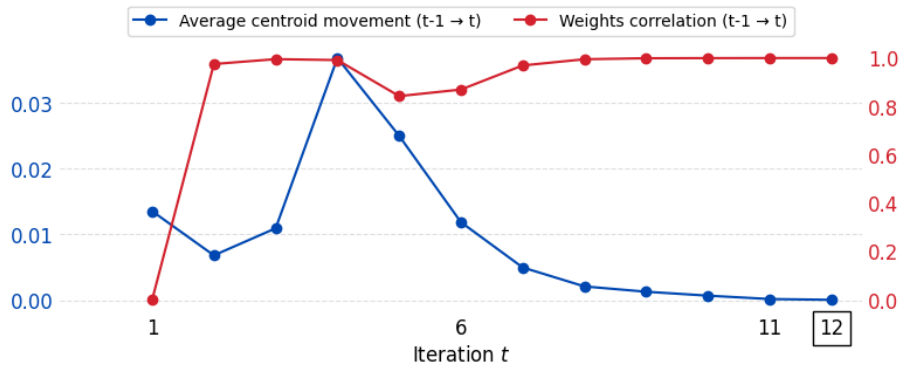
**Table C3:** Mean Adjusted Mutual Information (AMI) and Davies–Bouldin index (DB) values with 95%  $t$ -confidence intervals per dataset over runs. Gray ranges (—) show confidence intervals; best mean values are in **bold** (max for AMI, min for DB).

Dataset	Metric	$k$ -means	LOF $k$ -means	iLOF $k$ -means	OW $k$ -means	K-Std
MIP	AMI	0.414 0.401–0.426	0.412 0.399–0.426	0.422 0.412–0.433	0.411 0.398–0.425	<b>0.437</b> 0.427–0.447
	DB	0.801 0.728–0.873	0.819 0.739–0.900	0.839 0.758–0.920	0.773 0.712–0.833	<b>0.740</b> 0.674–0.805
WNE	AMI	0.837 0.789–0.885	0.853 0.807–0.899	0.841 0.793–0.889	0.833 0.798–0.868	<b>0.892</b> 0.890–0.893
	DB	1.417 1.345–1.490	1.448 1.365–1.531	1.414 1.345–1.484	1.422 1.354–1.489	<b>1.389</b> 1.389–1.390
BRC	AMI	0.542 0.532–0.551	0.545 0.542–0.548	0.541 0.539–0.543	0.541 0.531–0.552	<b>0.593</b> 0.593–0.593
	DB	1.317 1.314–1.321	1.320 1.317–1.322	1.321 1.321–1.322	1.316 1.313–1.320	<b>1.304</b> 1.304–1.304
HTR	AMI	0.442 0.387–0.497	0.423 0.382–0.465	0.442 0.387–0.497	0.391 0.386–0.395	<b>0.572</b> 0.571–0.573
	DB	0.992 0.896–1.088	1.024 0.951–1.096	0.991 0.895–1.088	1.072 1.067–1.077	<b>0.690</b> 0.689–0.691
VCL	AMI	0.160 0.146–0.173	0.165 0.150–0.179	0.160 0.146–0.174	0.164 0.153–0.176	<b>0.169</b> 0.155–0.182
	DB	0.856 0.769–0.944	0.848 0.768–0.927	0.856 0.769–0.944	0.854 0.778–0.929	<b>0.819</b> 0.757–0.880
SMS	AMI	0.343 0.343–0.343	0.343 0.343–0.343	0.343 0.343–0.343	0.328 0.327–0.329	<b>0.364</b> 0.364–0.364
	DB	4.068 4.068–4.069	4.068 4.068–4.068	4.068 4.068–4.068	4.130 4.127–4.134	<b>3.984</b> 3.983–3.984
MDS	AMI	0.867 0.854–0.879	0.878 0.868–0.888	0.869 0.857–0.881	0.868 0.854–0.881	<b>0.887</b> 0.874–0.899
	DB	1.904 1.853–1.955	1.891 1.852–1.930	1.885 1.834–1.935	1.911 1.858–1.963	<b>1.785</b> 1.749–1.821
INR	AMI	0.091 0.085–0.097	0.092 0.088–0.097	0.090 0.085–0.095	0.098 0.092–0.103	<b>0.102</b> 0.102–0.102
	DB	0.893 0.854–0.932	0.871 0.835–0.908	0.892 0.852–0.932	0.874 0.844–0.905	<b>0.836</b> 0.836–0.836
DBT	AMI	0.081 0.052–0.111	0.082 0.053–0.110	0.086 0.057–0.115	0.090 0.066–0.114	<b>0.107</b> 0.076–0.137
	DB	2.002 1.806–2.198	<b>1.998</b> 1.798–2.198	2.009 1.811–2.207	2.090 2.068–2.113	2.005 1.808–2.202
BBC	AMI	0.836 0.811–0.862	0.821 0.789–0.853	0.833 0.806–0.859	0.827 0.799–0.856	<b>0.839</b> 0.816–0.862
	DB	2.644 2.616–2.672	2.688 2.631–2.745	2.651 2.621–2.681	2.655 2.623–2.686	<b>2.636</b> 2.611–2.662
LKM	AMI	0.054 0.020–0.087	0.101 0.048–0.153	0.087 0.032–0.142	0.036 0.004–0.068	<b>0.112</b> 0.081–0.144
	DB	2.717 2.433–3.000	2.911 2.660–3.163	2.716 2.421–3.010	2.713 2.403–3.022	<b>2.634</b> 2.107–3.160
RE8	AMI	0.517 0.497–0.538	0.521 0.501–0.540	0.518 0.498–0.539	0.507 0.481–0.534	<b>0.525</b> 0.504–0.546

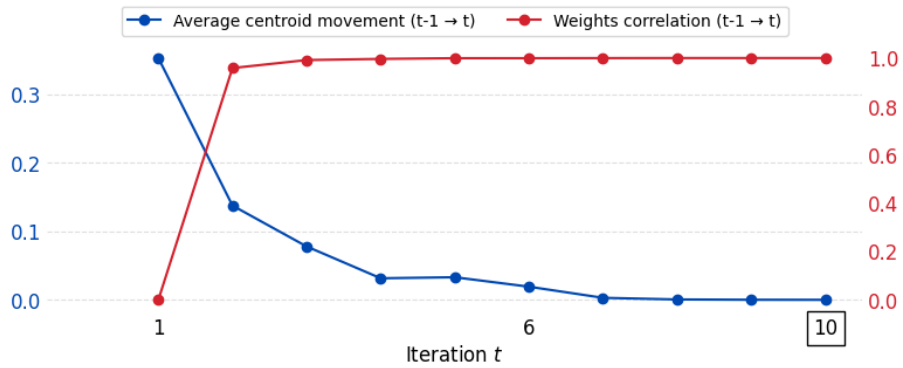
Dataset	Metric	<i>k</i> -means	LOF <i>k</i> -means	iLOF <i>k</i> -means	OW <i>k</i> -means	K-SIL
B77	DB	2.103 2.036–2.170	2.096 2.036–2.156	2.110 2.039–2.182	2.191 2.119–2.263	<b>2.048</b> 1.982–2.113
	AMI	0.718 0.713–0.722	0.716 0.714–0.719	<b>0.719</b> 0.714–0.723	0.716 0.712–0.720	<b>0.719</b> 0.715–0.723
	DB	1.718 1.688–1.747	1.735 1.720–1.749	1.728 1.697–1.759	1.749 1.719–1.779	<b>1.692</b> 1.667–1.716
CLC	AMI	0.841 0.840–0.843	0.841 0.839–0.842	<b>0.842</b> 0.841–0.844	0.837 0.836–0.839	<b>0.842</b> 0.841–0.844
	DB	2.027 2.015–2.039	2.012 2.000–2.025	2.033 2.021–2.044	2.055 2.044–2.066	<b>2.004</b> 1.994–2.013
STL	AMI	0.894 0.863–0.926	0.893 0.869–0.918	0.893 0.862–0.925	0.887 0.857–0.917	<b>0.899</b> 0.872–0.925
	DB	2.168 2.075–2.261	<b>2.118</b> 2.042–2.193	2.171 2.078–2.265	2.181 2.078–2.285	<b>2.127</b> 2.039–2.214



(a) Leukemia (LKM)

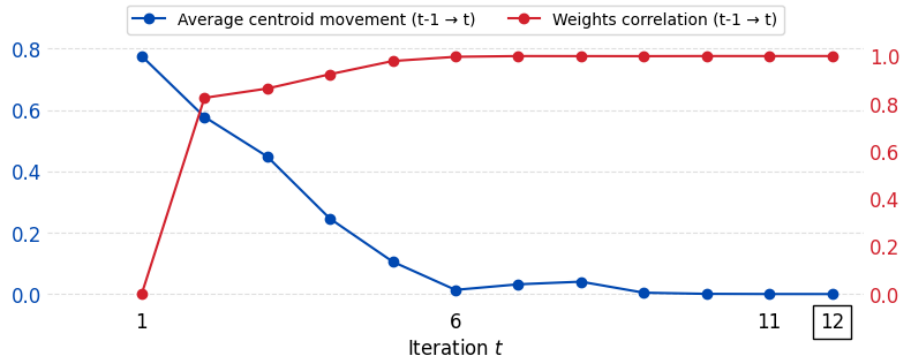


(b) Ionosphere (INR)

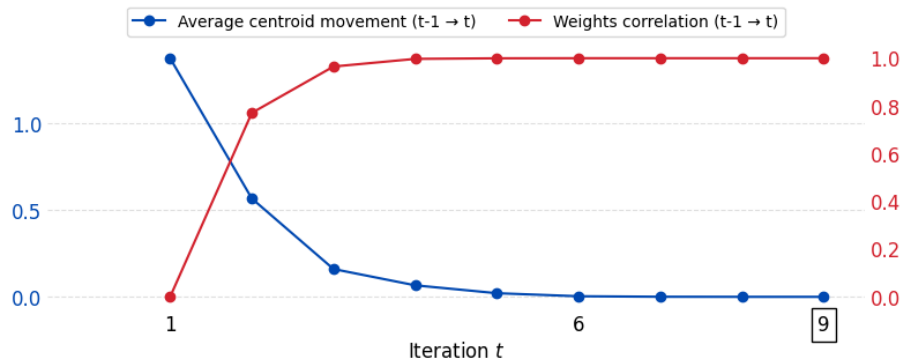


(c) Diabetes (DBT)

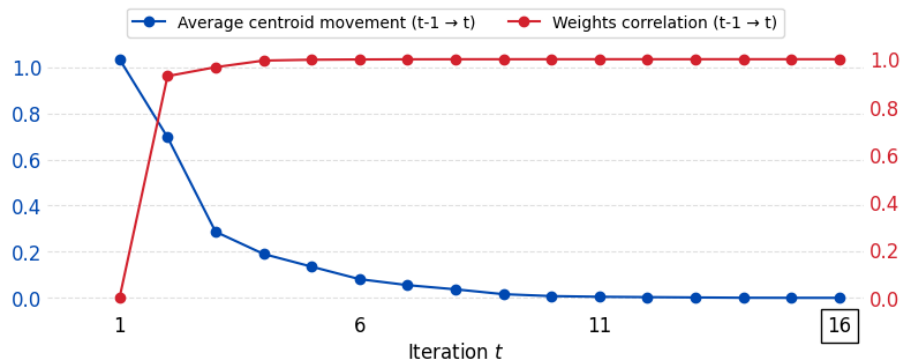
**Fig. C3:** Average centroid movement and weights correlation across K-SIL iterations  $t$  (§5.2) for LKM, INR, and DBT. The final iteration is marked by  $\square$ .



(a) Wine (WNE)

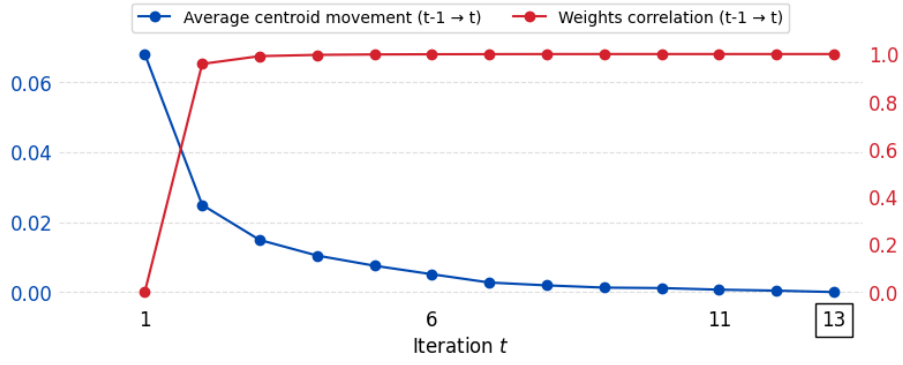


(b) Breast Cancer (BRC)

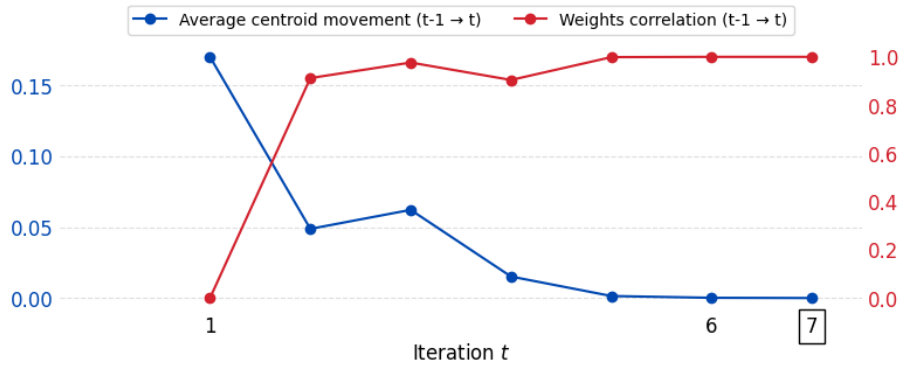


(c) HTRU2 (HTR)

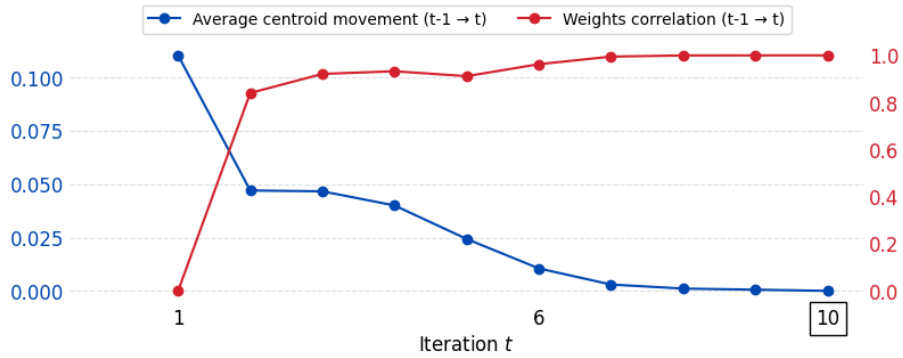
**Fig. C4:** Average centroid movement and weights correlation across K-SIL iterations  $t$  (§5.2) for WNE, BRC, and HTR. The final iteration is marked by □.



(a) SMS Spam (SMS)

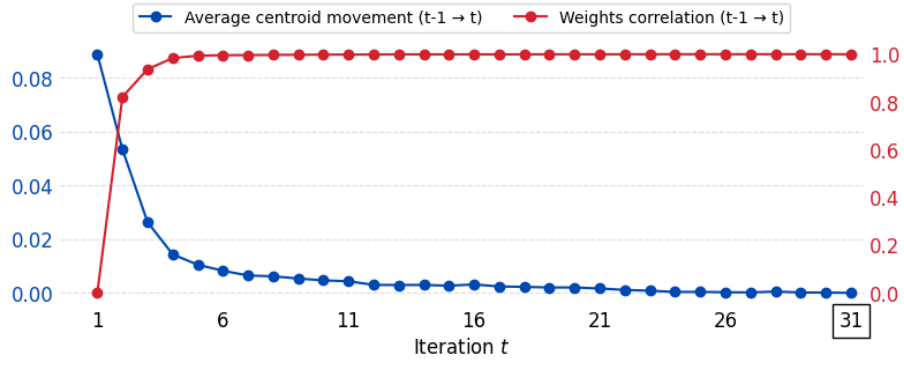


(b) MINDS-14 (MDs)

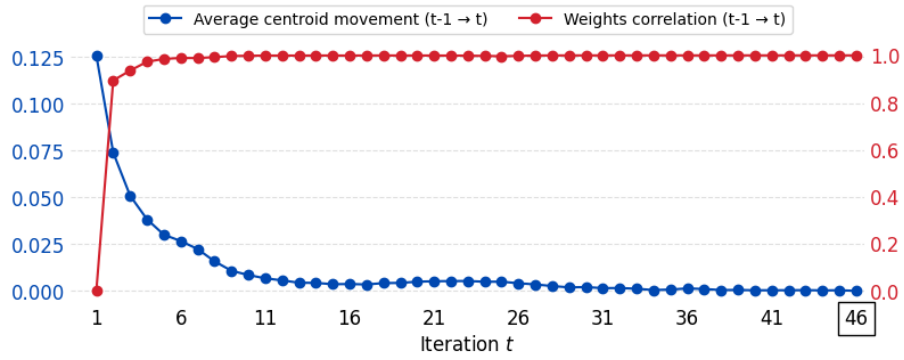


(c) BBC News (BBC)

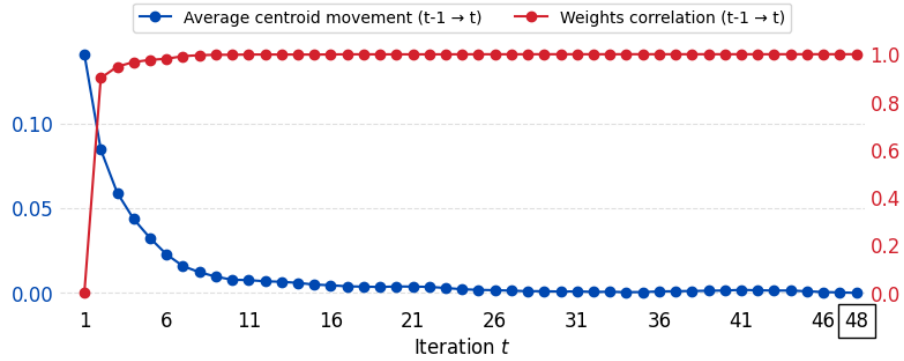
**Fig. C5:** Average centroid movement and weights correlation across K-SIL iterations  $t$  (§5.2) for SMS, MDS, and BBC. The final iteration is marked by  $\square$ .



(a) R8 (RE8)

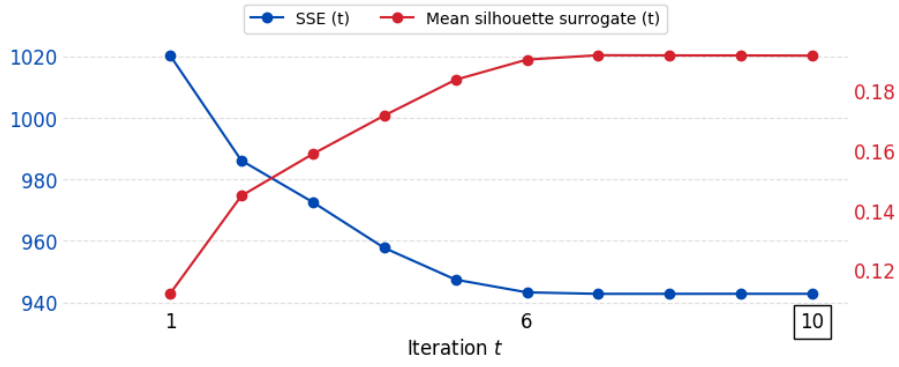


(b) Banking77 (B77)

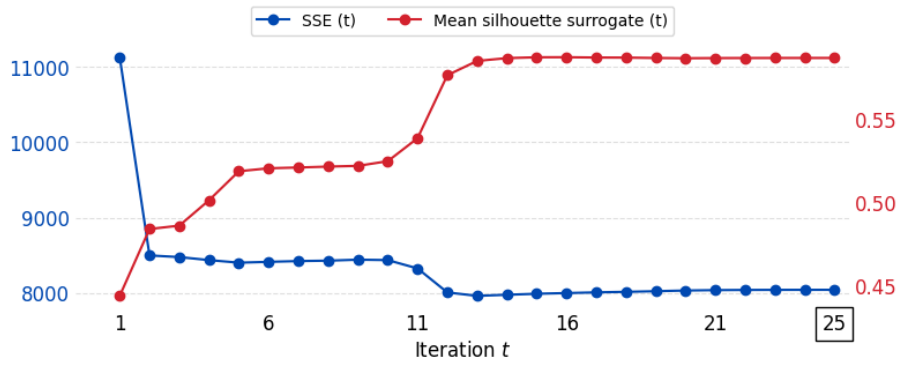


(c) CLINC150 (CLC)

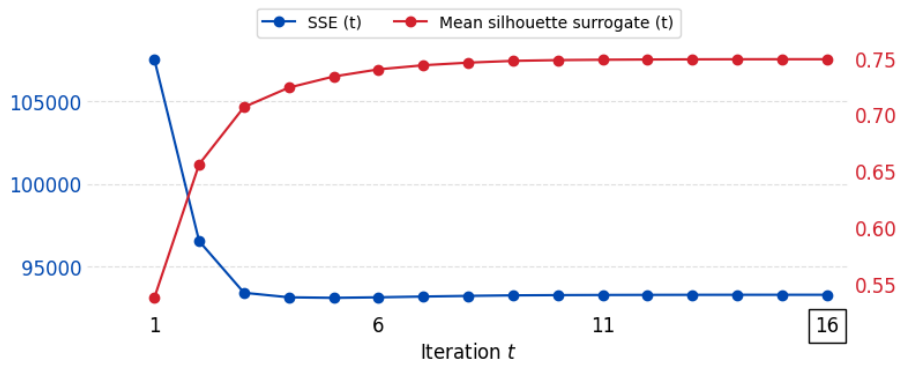
**Fig. C6:** Average centroid movement and weights correlation across K-SIL iterations  $t$  (§5.2) for RE8, B77, and CLC. The final iteration is marked by  $\square$ .



(a) BBC



(b) MIP



(c) HTR

**Fig. C7:** SSE and Silhouette score across K-SIL iterations  $t$  (§5.2) for representative datasets: BBC, MIP, and HTR. The final iteration is marked by  $\square$ .

## C.1 Initial temperature

To choose the warm-start temperature  $\tau_0$  (used only at the beginning of K-SIL), we inspect the distribution of the initialization silhouette-surrogate scores  $s_i(\mu_0)$  obtained right after the random initialization, before any reweighting or center updates. For each dataset we pool  $s_i(\mu_0)$  over multiple random seeds and summarize it with: (i) the median and interquartile range (IQR), and (ii) the boundary mass  $P[s_i(\mu_0) < 0.10]$ , i.e., the fraction of points that start in a low-confidence / ambiguous regime. Intuitively,  $\tau_0$  controls how sharply the initial reweighting separates points that look confidently assigned under the initial partition from points that look ambiguous. When  $\tau_0$  is larger, the early weights react more strongly to differences in  $s_i(\mu_0)$ , so points with higher initialization confidence are emphasized more at the warm start; when  $\tau_0$  is smaller, the warm start is milder and the method behaves closer to an unweighted start. Since this choice only affects the first stage, we restrict attention to a simple binary decision  $\tau_0 \in \{1, 2\}$ . Heuristically, we set  $\tau_0 = 2$  when the pooled initialization scores indicate that the initial partition contains either (i) a very large ambiguous mass, or (ii) a mixed confidence regime, or (iii) strongly heterogeneous confidence. Concretely, we choose  $\tau_0 = 2$  if any of the following holds: (i)  $P[s_i(\mu_0) < 0.10] \geq 0.90$ ; or (ii)  $\text{median}(s_i(\mu_0)) \in [0.15, 0.25]$  and  $P[s_i(\mu_0) < 0.10] \geq 0.20$ ; or (iii)  $\text{IQR}(s_i(\mu_0)) \geq 0.25$  and  $\text{median}(s_i(\mu_0)) \leq 0.50$ . Otherwise we use the milder warm start  $\tau_0 = 1$ . Table C4 reports these pooled initialization summaries and the resulting  $\tau_0$  choice for each dataset.

Dataset	Median	IQR	$P[s < 0.10]$	$\tau_0$
Sms	0.036	0.043	0.95	2
Clc	0.151	0.220	0.37	2
Mds	0.211	0.264	0.27	2
Lkm	0.182	0.161	0.23	2
Dbt	0.270	0.262	0.17	2
Wne	0.325	0.291	0.14	2
BrC	0.404	0.325	0.10	2
MiP	0.490	0.370	0.07	2
Bbc	0.084	0.107	0.57	1
Stl	0.131	0.160	0.40	1
Re8	0.136	0.186	0.39	1
B77	0.148	0.210	0.37	1
Htr	0.504	0.398	0.07	1
Vcl	0.563	0.325	0.06	1
Inr	0.583	0.296	0.05	1

**Table C4:** Initialization diagnostics (pooled over random seeds) and resulting warm-start choice  $\tau_0 \in \{1, 2\}$ .